

31 **Abstract**

32 As part of the second phase of the Regional Carbon Cycle Assessment and Processes project
33 (RECCAP2), we present an assessment of the carbon cycle of the Atlantic Ocean, including the
34 Mediterranean Sea, between 1985 and 2018 using global ocean biogeochemical models (GOBMs)
35 and estimates based on surface ocean carbon dioxide (CO₂) partial pressure (pCO₂ products) and
36 ocean interior dissolved inorganic carbon observations. Estimates of the Atlantic Ocean long-term
37 mean net annual contemporary CO₂ uptake based on GOBMs and pCO₂ products are in reasonable
38 agreement (-0.47 ± 0.15 PgCyr⁻¹ and -0.36 ± 0.06 PgCyr⁻¹, respectively), with the higher uptake in the
39 GOBM-based estimates likely being a consequence of a deficit in the representation of natural
40 outgassing of land derived carbon. In the GOBMs, the CO₂ uptake is increasing with time at rates
41 close to what one would expect from the atmospheric CO₂ increase, but pCO₂ products estimate a
42 rate twice as fast. The largest disagreement in the CO₂ flux between GOBMs and pCO₂ products is
43 found north of 50°N, coinciding with the largest disagreement in seasonal cycle and interannual
44 variability. The mean accumulation rate of anthropogenic CO₂ (C_{ant}) over 1994-2007 in the Atlantic
45 Ocean is 0.52 ± 0.11 PgC yr⁻¹ according to the GOBMs, $28 \pm 20\%$ lower than that derived from
46 observations. Around 70% of this C_{ant} is taken up from the atmosphere, while the remainder is
47 imported from the Southern Ocean through lateral transport.

48 **Plain Language Summary**

49 This study contributes to the second Regional Carbon Cycle Assessment and Processes by
50 presenting a carbon cycle evaluation of the Atlantic Ocean including the Mediterranean Sea between
51 1985 and 2018. The assessment draws on output from global ocean biogeochemical models along
52 with estimates based on observations of surface ocean carbon dioxide (CO₂) partial pressure (pCO₂
53 products) and ocean interior dissolved inorganic carbon. The models suggest that the Atlantic took
54 up -0.47 ± 0.15 Pg of carbon per year, in reasonable agreement with an uptake of -0.36 ± 0.06 Pg carbon
55 per year computed from pCO₂ products. In the models, the rate of CO₂ uptake is keeping pace with
56 the increase of atmospheric CO₂, but it is twice as fast in the pCO₂ products. Most of the uptake of
57 CO₂ by the ocean occurs in response to excess CO₂ released to the atmosphere from human activities.
58 The so-called anthropogenic carbon accumulates in the Atlantic Ocean at a rate of 0.52 ± 0.11 Pg
59 carbon per year according to the models. This estimate is $28 \pm 20\%$ lower than that derived from
60 observations. Further investigation reveals that about 70% of the accumulated anthropogenic carbon
61 is taken up from the atmosphere, while the remainder is imported from the Southern Ocean.

62

63 **1 Introduction**

64 During the International Geophysical Year 1957-58, Taro Takahashi (1930-2019) made the
65 first systematic and accurate measurements of carbon dioxide gas (CO₂) partial pressure in the air and
66 sea surface along an Atlantic Ocean transect from Greenland to Cape Town (Takahashi, 1961). Since
67 these early times, the importance of monitoring seawater CO₂ partial pressure (pCO₂) for the
68 assessment of sea-air exchanges of CO₂ has been increasingly recognized. Today, measurements of

69 pCO₂ have become an integral part of ocean monitoring programs including Eulerian time series
70 stations (Bates et al. 2014), oceanographic buoy arrays, and Ships of Opportunity (SOOP) programs
71 (Pfeil et al. 2013; Sabine et al. 2013; Bakker et al. 2016; Wanninkhoff et al. 2019). Early measurements
72 of pCO₂ highlighted spatial patterns that were confirmed later by time-series measurements (Keeling,
73 1993, Michaels et al., 1994, Bates et al., 1998, Gruber et al., 1998), large-scale data compilations and
74 the development of surface ocean CO₂ climatologies (Takahashi et al. 2002, Takahashi et al. 2009).
75 The North Atlantic between 25°N and 76°N stands out as a region of intense CO₂ uptake by the ocean.
76 It represents only 7% of the ocean surface, but accounts for 23% of the global uptake (Takahashi et
77 al. 2009; Schuster et al. 2013). Approximately two thirds of its contemporary uptake is caused by
78 natural processes, such as heat loss and export production, while the remaining one third is caused by
79 the increasing concentrations of CO₂ in the atmosphere and is therefore called uptake of
80 anthropogenic carbon, C_{ant} (Mikaloff-Fletcher et al. 2007; Gruber et al. 2009; Keeling et al. 1995;
81 Watson et al. 1995). The local uptake of C_{ant} by sea-air exchange in the Atlantic combined with the
82 net northward transport of C_{ant}-rich southern latitude waters by the upper limb of the Atlantic
83 meridional overturning circulation (AMOC) (McDonald et al. 2003; Roson et al. 2003; Perez et al.
84 2013; Brown et al. 2021) leads to a high accumulation of C_{ant} throughout the water column of the
85 Atlantic, accounting for approximately 35% of the global total storage (Sabine et al. 2004; Gruber et
86 al. 2019). Earlier studies highlighted the role of the AMOC, a key component of the global ocean
87 circulation and a distinctive dynamic element of the Atlantic circulation, in the redistribution of CO₂
88 (Holfort et al., 1998; Wallace, 2001). The AMOC further links the upper ocean thermohaline
89 circulation with the intense Deep Western Boundary Current (DWBC) connecting the waters formed
90 in the subpolar North Atlantic with the Southern Ocean (Haine et al. 2016, Hirschi et al. 2020, Rhein
91 et al. 2015). The DWBC contributes to natural interhemispheric carbon exchanges by transporting
92 between 0.5 and 1 PgC yr⁻¹ from North Atlantic uptake regions southward (Aumont et al 2001;
93 Macdonald et al. 2003; Resplandy et al 2018).

94 As part of the second phase of the Regional Carbon Cycle Assessment and Processes project
95 (RECCAP2), we complement these earlier studies about the Atlantic carbon budget with an analysis
96 of the latest observation- and model-based estimates of the Atlantic Ocean including sea-air fluxes
97 (natural and anthropogenic), storage, and transport of CO₂ for the years 1985 to 2018. Following Fay
98 and McKinley (2014), RECCAP2 divides the Atlantic into five regions or biomes (Figure 1a), namely
99 the North Atlantic subpolar gyre (NA SPSS), the seasonally and permanently stratified regions of the
100 North Atlantic subtropical gyre (NA STSS and NA STPS), the Atlantic equatorial upwelling region
101 (AEQU), and the permanently stratified South Atlantic subtropical gyre extending southward to
102 ~35°S (SA STPS). The Mediterranean Sea is also included as a single, sixth biome (MED). Among
103 these regions, the NA SPSS stands out as a biome with a high spatial and temporal variability, which
104 still challenges our understanding, assessments, and modeling efforts despite the increase in
105 observational capacity over the last two decades. During the RECCAP1 period (1990-2009), Schuster
106 et al. (2013) estimated an average CO₂ uptake of -0.21 ± 0.06 PgC yr⁻¹ (**positive sign indicating flux**
107 **into the atmosphere (outgassing), and negative sign a flux into the ocean (uptake)**) between 49°N
108 and 79°N, consistent across observation-based estimates and numerical models used. This flux

109 amounts to 10% of the global uptake and makes the NA subpolar region one of the regions with the
110 highest CO₂ uptake density (see Suppl-Info Text 1). Understanding the seasonal, interannual and
111 long-term variability of the high latitude Atlantic CO₂ sink has been the focus of many observational
112 and modeling studies (e.g., Thomas et al., 2008; Ullman et al., 2009; Watson et al., 2009; Tjiputra et
113 al., 2012; Goris et al., 2015; Breeden and McKinley, 2016; Lesseure et al., 2020; Macovei et al.,
114 2020). It has become clear that the variability of sea-air fluxes of CO₂ and C_{ant} storage rates in this
115 region is influenced by regional modes of climate variability, such as the North Atlantic Oscillation
116 (NAO), through its effect on wind patterns and ocean heat loss, mixing, and deep water formation.
117 During the time period from the 1990s to the 2000s, C_{ant} storage rates decreased in the subpolar NA
118 in response to the shift from predominantly high (1990 to 1995) to low (2002 to 2007) NAO (Perez
119 et al., 2008, Steinfeldt et al., 2009, Perez et al., 2013; Gruber et al., 2019). As part of their global
120 assessment, Müller et al. (2023) found that only the North Atlantic exhibited a trend towards weaker
121 C_{ant} accumulation relative to the atmospheric CO₂ increase by comparing their inventory changes
122 from 2004 to 2014 and from 1994 to 2004 with previous estimates for the period 1800 to 1994 from
123 Sabine et al. (2004). However, recent observations show a reinvigoration of the C_{ant} accumulation at
124 local scale associated with increased convection in the mid 2010s (Fröb et al., 2016), as a consequence
125 of a shift back to positive NAO conditions.

126 The subtropical North Atlantic (in RECCAP1 defined to be 18° to 49°N, 7.2% of the ocean
127 surface, see Suppl-Info Text 1) was shown to be a CO₂ sink, with a net uptake of -0.26 ± 0.06 PgC yr⁻¹
128 between 1990 and 2009 (Schuster et al. 2013), due in approximately equal parts to C_{ant} and natural
129 CO₂ uptake, where the latter is driven mainly by net heat loss, with limited contributions from
130 biological activity (Gruber et al., 2009). The mean subtropical gyre uptake rate (-0.91 mol C m⁻² yr⁻¹)
131 is similar to that observed at the Bermuda Atlantic Time-series Study (Bates et al. 2014), even
132 though the eastern return branch of the subtropical gyre showed lower uptake values (Santana-
133 Casiano et al., 2007). At both sites, the interannual variability of CO₂ flux correlates with sea surface
134 temperature (SST) and mixed layer depth anomalies (González-Dávila et al., 2010; Gruber et al.,
135 2002; Santana-Casiano et al., 2007). SST is the main driver of the seasonal cycle in the subtropics,
136 driving an outgassing of CO₂ in summer and uptake in winter.

137 The tropical Atlantic is the second largest oceanic source of CO₂ to the atmosphere, after the
138 tropical Pacific, with an annual emission of 0.10-0.11 PgC yr⁻¹ (Takahashi et al., 2009; Landschützer
139 et al., 2014) due to frequent upwelling of cold, CO₂-rich water in the eastern parts. Based on six
140 different methodologies, the RECCAP1 estimate for this region converged on an outgassing of
141 0.12 ± 0.04 PgC yr⁻¹ between 1990 and 2009 (Schuster et al., 2013; see Suppl-Info Text 1). The
142 increase in atmospheric CO₂ has decreased the net outgassing since preindustrial times, as the ocean
143 supersaturation is reduced by about 50% (Gruber et al., 2009). This implies an uptake of
144 anthropogenic CO₂. Gruber et al. (2009) also suggested that an important part of this natural
145 outgassing is due to the riverine contribution of organic matter, especially that stemming from the
146 Amazon river (Louchard et al., 2021).

147 The subtropical South Atlantic is a sink for atmospheric CO₂ (Schuster et al., 2013;

148 Rödenbeck et al., 2015), driven in almost equal parts by natural and anthropogenic CO₂ fluxes
149 (Gruber et al., 2009). It has been suggested that strong upwelling events in the eastern part generate
150 significant interannual variability (Schuster et al., 2013; see Suppl-Info Text 1). However, pCO₂
151 variability in the SA STPS biome is relatively low as shown by Rodenbeck et al. (2015). From 1990
152 to 2009, this region was a CO₂ sink of -0.14 ± 0.04 PgC yr⁻¹ on average, combining areas with a net
153 outgassing north of the 23°C isotherm (Ito et al., 2005) with areas of absorption to the south. This
154 region is relatively poorly sampled with the domain north of 31°S acting as a source in spring and
155 sink in autumn (Santana-Casiano et al., 2007; González-Dávila et al., 2009; Padín et al., 2010).
156 Estimates of long-term CO₂ flux trends in this region are highly dependent on the methodology used
157 (Schuster et al., 2013).

158 The Mediterranean Sea represents 3.5% of the Atlantic Ocean area and is the only mid-latitude
159 ocean basin in which deep convection occurs (see Suppl-Info Text 1). This circulation is responsible
160 for a relatively large inventory of C_{ant} of 1.7 PgC in 2001 as estimated from CFCs (Schneider et al.,
161 2010). The overturning time is fast in relation to that of the global ocean (60 to 220 years vs more
162 than 1000 years; Stöven and Tanhua, 2014; Khatiwala et al., 2013) and allows a complete renewal of
163 water in the basin on a centennial time scale. Hence, surface waters enriched in C_{ant} transfer this
164 signature to deep layers relatively quickly, leading to all water masses in the basin being already
165 invaded by C_{ant} (Hassoun et al., 2015). However, surface pCO₂ exhibits large variability, due to the
166 large heterogeneity of physical and trophic regimes in the two main Mediterranean sub-basins, with
167 a marked west-to-east oligotrophy gradient and different atmospheric forcings that regulate seawater
168 pCO₂ and the sea-air CO₂ exchanges (Krasakopoulos et al., 2009; 2017, Ingrosso et al., 2016, Urbini
169 et al., 2020, De Carlo et al., 2013; Kapsenberg et al., 2017, Petihakis et al., 2018, Sisma-Ventura et
170 al., 2017, Coppola et al., 2018, Wimart-Rousseau et al., 2021).

171 In RECCAP1, the assessment of the ocean carbon cycle relied on five global ocean
172 biogeochemical models (GOBMs), several atmospheric and oceanic inversions, the pCO₂
173 climatology published by Takahashi et al (2009), as well as the SOCAT (Surface Ocean CO₂ Atlas)
174 database. A crucial progress since RECCAP1 are annual updates of SOCAT (Bakker et al., 2016),
175 with over 33.7 million quality-controlled surface ocean pCO₂ measurements in the 2022 release
176 (Bakker et al., 2022). The availability of these data sparked the development of time-varying
177 reconstructions of surface ocean pCO₂ distributions. These pCO₂ products rely on advanced statistical
178 techniques and neural networks to extrapolate sparse observations in time and space to achieve
179 temporally resolved global coverage (e.g., Landschützer et al, 2014, Rödenbeck et al., 2014, Gregor
180 et al., 2019, Chau et al., 2022). Similarly, advances in biogeochemical modeling since RECCAP1 led
181 to the contribution of an increased number of GOBMs that provided output from up to four different
182 simulations allowing to disentangle the natural carbon cycle and the anthropogenic perturbation
183 (Wanninkhof et al., 2013, Friedlingstein et al., 2022).

184 Improved process understanding and increasing availability of ocean biogeochemical data
185 have led to advances in GOBMs, particularly in simulating the large-scale features and mean state of
186 the ocean carbon cycle (Seferian et al., 2020). When forced with atmospheric reanalysis and

187 atmospheric CO₂ concentration data, these models were assessed to be suitable in quantifying the
188 global ocean carbon fluxes, from annual mean to interannual time-scale (Hauck et al., 2020).
189 Regionally, such models have also been shown to be capable of simulating the observed long-term
190 pCO₂ trends (Tjiputra et al., 2014). Nevertheless, some GOBMs still have difficulties in representing
191 the observed seasonal cycle in key ocean sink regions in the North Atlantic, likely owing to mismatch
192 in the timing of deep winter mixing and/or biological bloom events (Tjiputra et al., 2012; Schwinger
193 et al., 2016). Since RECCAP1, the number of GOBMs has increased from six to eleven in RECCAP2,
194 and while not all RECCAP1 models participated in the RECCAP2 exercise, those that do have likely
195 gone through iterations of improvements (the readers are referred to Supplementary Table S1 in
196 DeVries et al., 2023, for individual biogeochemical model descriptions). In the Atlantic domain,
197 recent developments in the ocean physical component have led to better representation of large scale
198 circulation and ventilation processes (Hirschi et al. 2020), which could have strong implications on
199 the transports of biogeochemical tracers driving the sea-air CO₂ fluxes and interior carbon
200 sequestration in this basin.

201 This synthesis paper is structured as follows. Section 2 provides the details of the database
202 consisting of data sets based on observations of both surface pCO₂ and the marine carbonate system
203 in the ocean interior, and an ensemble of global biogeochemical models together with a regional
204 model and an assimilation model. In Section 3, the CO₂ fluxes obtained for each class of products are
205 described and analyzed considering both the mean values for the study period, trends in two periods
206 (1985-2000 and 2000-2018), the seasonal cycle and the interannual variability of CO₂ fluxes. In
207 addition, the accumulation of anthropogenic CO₂ in the ocean interior is evaluated. In section 4, we
208 discuss the results obtained in RECCAP2 in comparison to RECCAP1, as well as the consistency and
209 discrepancies between the global biogeochemical models and different data products, and suggest
210 ways for future improvements. Section 5 summarizes the main conclusions and lists some of the
211 remaining challenges to be solved in future versions of RECCAP.

212 **2 Methods**

213 The Atlantic Ocean and its subdivision into biomes is defined by the RECCAP2 basin mask
214 (Müller, 2023) that builds on the biome definition by Fay and McKinley (2014) and extends from
215 approximately 79°N to approximately 35°S (Figure 1). The RECCAP2 ocean database used in this
216 study is described in DeVries et al. (2023), consisting of observation-based and model-based
217 products. Here, we use two types of observation-based products, namely surface ocean pCO₂ (pCO₂
218 products) and ocean interior C_{ant} reconstructions. For model-based products, we use Global and
219 Regional Ocean Biogeochemical Model (GOBM/ROBM) hindcast simulations and an ocean data-
220 assimilation model. All products have been re-gridded onto a common 1°×1° horizontal grid and
221 monthly temporal resolution by the data providers, except for ocean interior model outputs which
222 were submitted as annual averages. Ocean model outputs were either provided on the models'
223 standard depth levels or re-gridded to fixed depth levels chosen by the data providers.

224 2.1. Observation-based products

225 2.1.1 $p\text{CO}_2$ products

226 This analysis draws on a variety of observation-based products for surface ocean $p\text{CO}_2$ and
 227 sea-air CO_2 fluxes (Table S1). These products are based on the interpolation of in situ $p\text{CO}_2$ data
 228 accessed from different releases (v2019-v2021, v5) of SOCAT (Bakker et al., 2016) to near-global
 229 coverage. Several interpolation methods are used including machine learning techniques
 230 (Landschützer et al., 2014; Gregor et al., 2019; Watson et al., 2020; Chau et al., 2022; Gloege et al.,
 231 2021; Gregor and Gruber, 2021; Iida et al., 2021, Zeng et al., 2022) and a diagnostic mixed layer
 232 scheme (Rödenbeck et al., 2013). Sea-air CO_2 fluxes (FCO_2) are computed from reconstructed $p\text{CO}_2$
 233 fields following:

$$234 \quad \text{FCO}_2 = K_w (1-f_{\text{ice}}) K_0 (p\text{CO}_2 - p\text{CO}_{2,\text{air}}) \quad (1)$$

235 where: K_w is gas transfer velocity; f_{ice} is sea-ice cover fraction; K_0 is CO_2 solubility in seawater; and
 236 $p\text{CO}_2$, and $p\text{CO}_{2,\text{air}}$ are the partial pressures of CO_2 in seawater (nominally at 5 m depth) and in the
 237 overlying atmosphere, respectively. The gas transfer velocity is computed as a function of wind speed
 238 at 10 m mostly assuming a quadratic relationship (Wanninkhof, 1992; 2014, Nightingale et al., 2000;
 239 Ho et al. 2006). For the set of $p\text{CO}_2$ products, the uncertainty of the mean is determined as the standard
 240 deviation of the FCO_2 of the nine $p\text{CO}_2$ products referenced in Table S1.

241 The $p\text{CO}_2$ product by Watson et al. (2020), UOEX-Wat20, is different from the other products
 242 as it adjusts the underlying $p\text{CO}_2$ observations accounting for the cool-skin effect and for near-surface
 243 temperature gradients following Goddijn-Murphy et al. (2015) and Woolf et al. (2016), henceforth
 244 referred to as the surface skin effects. While it applies the SOMFFN interpolation approach also used
 245 in MPI-SOMFFN it does so in different fashion such that the differences in the UOEX-Wat20 and
 246 other approaches are not solely attributed to adjusting the $p\text{CO}_2$ values. While UOEX-Wat20 is
 247 included in the analysis, it is kept distinct from the other nine $p\text{CO}_2$ products, because of the difference
 248 in approach.

249 The $p\text{CO}_2$ products all use the bulk flux parameterization (equation 1) and aside from UOEX-
 250 Wat20 follow the convention of reference depth for $p\text{CO}_2$ at nominally 5-m. Uncertainty estimates
 251 provided here are mainly based on differences between the different products. Uncertainties and
 252 biases in gas transfer velocities, and impacts of near- surface $p\text{CO}_2$ gradients (Dong et al., 2022;
 253 Bellenger et al., 2023) are not taken into account but are estimated to increase the uncertainty in the
 254 $p\text{CO}_2$ products by 3-fold on global scales (See Table 3, DeVries et al., 2023).

255 2.1.2 Ocean interior C_{ant} reconstructions

256 Furthermore, we consider two ocean interior observation-based products, one based on
 257 measurements of dissolved inorganic carbon (DIC) concentrations collected over more than 30 years,
 258 and other physical and biogeochemical parameters by Gruber et al. (2019), and another one
 259 combining an inversion approach with tracer measurements by Khatiwala et al. (2009). The Gruber
 260 et al. (2019) product provides an estimate of the ocean C_{ant} storage change (ΔC_{ant}) between the years

261 1994 and 2007. This estimate is based on the eMLR(C*) method (Clement and Gruber, 2018) applied
262 on the GLODAPv2 data (Olsen et al., 2016). It includes estimates from surface to 3000 m depth for
263 both the steady-state and non-steady-state components of ΔC_{ant} in the ocean interior. In the North
264 Atlantic and below 3000 m, Gruber et al. (2019) estimated an inventory change C_{ant} of 0.05 PgC yr-
265 1 (~8% of the accumulation above 3000 m), which has been proportionally distributed across biomes
266 according to the GOBM ΔC_{ant} below 3000 m. The product from Khatiwala et al. (2009) provides
267 estimates of the increase of the oceanic C_{ant} content from 1850 up to 2011 and is based on a Green's
268 Function approach that allows a gradual increase in the CO₂ disequilibrium between the atmosphere
269 and the ocean.

270 The C_{ant} reconstruction product from Khatiwala et al. (2009) was pre-processed to match the
271 RECCAP2 1°×1° grid and depth levels of the ΔC_{ant} reconstruction from Gruber et al. (2019). Since
272 the product provides annual values, we calculated ΔC_{ant} between 1994-2007 to allow for comparison
273 with Gruber et al. (2019). The ΔC_{ant} reconstruction of Gruber et al. (2019) does not cover the entire
274 NA SPSS biome explored in our study, so we extrapolated the product to the Nordic Seas assuming
275 the same vertical ΔC_{ant} profile as at 65°N, resulting in a 23% increase of ΔC_{ant} storage rate in the NA
276 SPSS biome. The percentage of increase obtained was applied to Khatiwala et al. (2009), as it also
277 does not fully cover the NA SPSS biome. The uncertainty in C_{ant} inventory increase in each biome
278 was estimated by surface scaling of the uncertainties of the North and South Atlantic provided by
279 Gruber et al. (2019). For the Khatiwala et al. (2009) product a relative uncertainty of 17% was set
280 following Khatiwala et al. (2013).

281 2.2 Global ocean biogeochemical models

282 As an improvement from RECCAP1 (Wanninkhof et al., 2013), the RECCAP2 protocol
283 provides a set-up of four simulations with four combinations of atmospheric physical and CO₂
284 concentration forcings such that the simulated total CO₂-fluxes can be divided into its steady-state
285 and non-steady state natural and anthropogenic components: (i) Simulation A: temporally varying
286 atmospheric reanalysis forcing and increasing atmospheric CO₂, (ii) Simulation B: climatological
287 atmospheric forcing and constant preindustrial atmospheric CO₂, (iii) Simulation C: climatological
288 atmospheric forcing and increasing atmospheric CO₂, and (iv) Simulation D: temporally varying
289 atmospheric reanalysis and constant preindustrial CO₂.

290 We used outputs from 11 GOBMs of which the majority also contributed to the Global Carbon
291 Budget (Friedlingstein et al., 2020; Supplementary Table S2). All GOBMs used here are general
292 ocean circulation models with coupled ocean biogeochemistry, run in hindcast mode and hence forced
293 by atmospheric data sets. Details of the respective model resolutions, forcings, and references are
294 provided in an overview table in DeVries et al. (2023). All models performed four simulations (A, B,
295 C, and D), except for MOM6-Princeton (not C and D). Additionally, we considered the output from
296 the regional ocean biogeochemical model (ROBM) ROMS-AtlanticOcean-ETHZ (Louchard et al.,
297 2021) that only performed Simulation A. We also included results from the ocean data-assimilation
298 model OCIMv2021 (DeVries et al., 2022) that performed simulations A, B and C. OCIMv2021 uses
299 a climatological mean circulation but has time-varying SST. It includes an abiotic carbon cycle model

300 forced with atmospheric CO₂ to estimate the anthropogenic carbon distribution.

301 To determine the FCO₂ for the period 1985-2018, for each GOBM and each biome, we
302 subtracted the linear trend of the respective fluxes estimated in Simulation B from Simulation A, to
303 correct for potential model-dependent drift. For the ensemble of GOBMs, the uncertainty of the mean
304 was determined as the standard deviation of the 11 models referenced in Table S2.

305 In order to be consistent with the ΔC_{ant} reconstruction of Gruber et al. (2019), the C_{ant}
306 accumulation rate in the GOBMs was evaluated between 1994 and 2007. Here, C_{ant} was calculated
307 as the difference in DIC between the simulation with increasing atmospheric CO₂ concentrations
308 (Simulation A) and the one with constant preindustrial atmospheric CO₂ concentrations (Simulation
309 D), both with time-varying atmospheric physical forcing. We considered all GOBMs that ran
310 Simulation A and Simulation D (Supplementary Table S2). However, MPIOM-HAMOCC was
311 excluded from the final analysis because of its large negative C_{ant} values in the interior due to the
312 inconsistent physical forcing between its Simulations A and D. For the OCIMv2021 model, C_{ant} was
313 determined as the difference between Simulations C (increasing atmospheric CO₂, climatological
314 atmospheric forcing) and B (constant preindustrial atmospheric CO₂, climatological atmospheric
315 forcing), as this model uses a steady-state circulation and did not run Simulations D. Once we
316 obtained the total C_{ant} concentrations from all GOBMs, we computed the C_{ant} storage changes as the
317 difference between the concentrations in 1994 and 2007. C_{ant} concentration changes were vertically
318 integrated to get the column inventory storage changes, as well as biome-integrated ΔC_{ant} rates. For
319 the GOBM ensemble, the uncertainty of the mean ΔC_{ant} rate is determined as the standard deviation
320 of the ΔC_{ant} rates of the nine models referenced in Table S2.

321 2.3. Area Coverage

322 Practically all pCO₂ products considered have a spatial coverage of almost 100% of the
323 Atlantic basin, except JMA-MLR and MPI-SOMFFN with about 91-92% of area coverage in the
324 northernmost biome (NA SPSS). Here, pCO₂ product fluxes were not scaled to the same ocean area,
325 following the assumption of Hauck et al. (2023), that the discrepancy arising from differences in
326 covered area are smaller than the uncertainty arising from any extrapolation to an equal area. All
327 GOBMs cover more than 98% of the area, except MPIOM-HAMOCC (95%) and CESM-ETHZ
328 (97%). ROMS-ETHZ (ROBM) covers 95% of the Atlantic Region, and only 93% of the NA SPSS
329 biome and 25% of the Mediterranean Sea. Likewise, most of the missing coverage of the MPIOM-
330 HAMOCC is located in the Mediterranean Sea, thus ROMS-ETHZ and MPIOM-HAMOCC have not
331 been used for the evaluation of the MED biome.

332 2.4 Riverine carbon outgassing

333 The flux of natural CO₂ across the sea-air interface includes also a flux balancing the input of
334 inorganic and organic carbon at the land-sea interface minus the fraction buried in marine sediments
335 (Regnier et al., 2012, Sarmiento and Sunquist, 1992). We refer to this flux component as preindustrial
336 riverine CO₂ outgassing (RCO). Since pCO₂ products are based on real-world observations, they
337 provide estimates of total FCO₂, including the RCO. In contrast, RCO is not at all or not adequately

338 represented in GOBMs. Its approximation would require several thousands of years of integration
339 with a GOBM including a sediment module. None of the GOBMs used here includes such a long
340 preindustrial spin-up (Terhaar et al., 2024). Though several of the GOBMs analyzed in this study
341 include river inputs of carbon, not all processes relevant for the land-sea flux are adequately
342 represented. In consequence, the average of the global imbalance between river input and flux to the
343 sediment is small ($<0.14 \text{ PgC yr}^{-1}$) in the GOBM ensemble (Terhaar et al., 2024) compared to the
344 observation-based global integral of RCO recommended in the RECCAP2 protocol, that amounts to
345 $0.65 \pm 0.3 \text{ PgC yr}^{-1}$ (Regnier et al., 2022). Combining the spatial distribution of RCO by Lacroix et
346 al. (2020) and the globally integrated estimate by Regnier et al. (2022) allows us, in principle, to
347 estimate its contribution to FCO_2 at biome scale, albeit with a relative uncertainty that is most likely
348 even larger than that of the global integral ($>50\%$ of the absolute value) and without considering the
349 already-present land-sea fluxes of the GOBMs. However, the magnitude of RCO is a major source of
350 uncertainty and hinders the straightforward comparison of fluxes from pCO_2 products and GOBMs.
351 In our analysis, we chose not to add the estimated RCO to the GOBMs but to present it separately,
352 whenever this is meaningful. As the RCO spatial distribution by Lacroix et al. (2020) is uncertain,
353 we do not apply it on a grid scale but only at biome scale.

354 **3 Results**

355 3.1 Sea-air CO_2 fluxes

356 *3.1.1 Long-term mean fluxes from 1985 to 2018: Spatial patterns and regional integrals*

357 The mean sea-air CO_2 fluxes of the pCO_2 products and GOBMs have very similar spatial
358 patterns when averaged over the 1985 to 2018 period (Figure 1c,d). The pCO_2 products show a weak
359 CO_2 outgassing over large areas of the tropical regions of the South and North Atlantic, which is more
360 intense in the western equatorial Atlantic. In comparison, the GOBMs exhibit weaker CO_2 fluxes in
361 the equatorial region but more intense CO_2 fluxes in the Benguela and Mauritanian upwelling areas.
362 In these upwelling regions, the ocean circulation delivers nutrients and DIC to the surface layer where
363 they are consumed by photosynthesizing organisms. In many of these regions, the supply of DIC from
364 below exceeds the amount of DIC being drawn down by the net balance between photosynthesis and
365 remineralization/respiration, i.e., net community production, such that an excess of DIC and nutrients
366 remain at the surface, indicative of an inefficient biological pump (Sarmiento and Gruber, 2006). As
367 a result, these regions act as a source of CO_2 to the atmosphere. Downstream of many of these regions,
368 the remaining nutrients and the DIC get drawn down completely. This resulting large increase in the
369 biological pump efficiency makes these regions strong uptake regions. The NA SPSS and NA STSS
370 biomes, and the southern parts of biome SA STPS are characterized by strong CO_2 uptake with some
371 differences between the spatial patterns modeled in the GOBMs and those derived from observations.
372 In these regions both the cooling of the warm poleward moving waters and an efficient and strong
373 biological pump promote CO_2 uptake from the atmosphere (Watson et al. 1995, Thomas et al. 2008,
374 Takahashi et al. 2009).

375 pCO_2 products and GOBMs are in good agreement with respect to their zonally integrated

376 CO₂ fluxes when regarding the northern hemisphere between equator and 40°N and the southern
377 hemisphere south of 20°S (Figure 1b). The GOBMs show a more intense ocean uptake of CO₂,
378 coinciding with the deep convection regions in the subpolar gyre (NA SPSS biome). In this region,
379 models underestimate the transport and mixing of high subsurface DIC water to the surface during
380 winter, underestimating the winter-time outgassing from the ocean (McKinley et al 2018). The results
381 obtained with the ROBM are very similar to that of the GOBMs between 35°S and 52°N, while it
382 seems to overestimate uptake north of 52°N even more than the GOBMs. The inverse model
383 OCIMv2021 follows the large-scale pattern of the other products, but shows more meridional
384 variations and, similar to the ROBM, it also simulates a much stronger uptake than seen in models
385 and observations north of 52°N (Figure 1b).

386 As shown in Figure S1, the SOCAT gridded data of pCO₂ covers the NA SPSS biome with
387 the highest number of observations among the Atlantic biomes, resulting in an average of 10.2% of
388 the maximum possible coverage since 2003 and making it one of the regions where the pCO₂ products
389 are expected to provide comparative robust results. The UOEX data product, that adjusts the pCO₂
390 for near-surface temperature and salinity gradients, shows higher CO₂ uptake than the ensemble mean
391 of the other pCO₂ products between 35°S and 50°N. This difference contains the expected effect of
392 lower skin temperature on solubility, for which adjustments have been made in the UOEX product,
393 but it also inherits the influence of different gap filling methods. Dong et al. (2022) have globally
394 reevaluated the effect of skin temperature on FCO₂ showing an impact on FCO₂ that is 30% lower
395 than that previously evaluated by Watson et al. (2020). The net effect of skin SST and salinity on
396 FCO₂ integrated over the whole Atlantic and its five biomes is detailed in Supplementary Table S4.
397 The change in CO₂ uptake due to the temperature effects estimated by Dong et al. (2022) is overall
398 similar to the difference in FCO₂ between UOEX and the ensemble mean of nine pCO₂ products
399 except for NA SPSS and SA STPS, where the different gap-filling methodology has a greater effect.

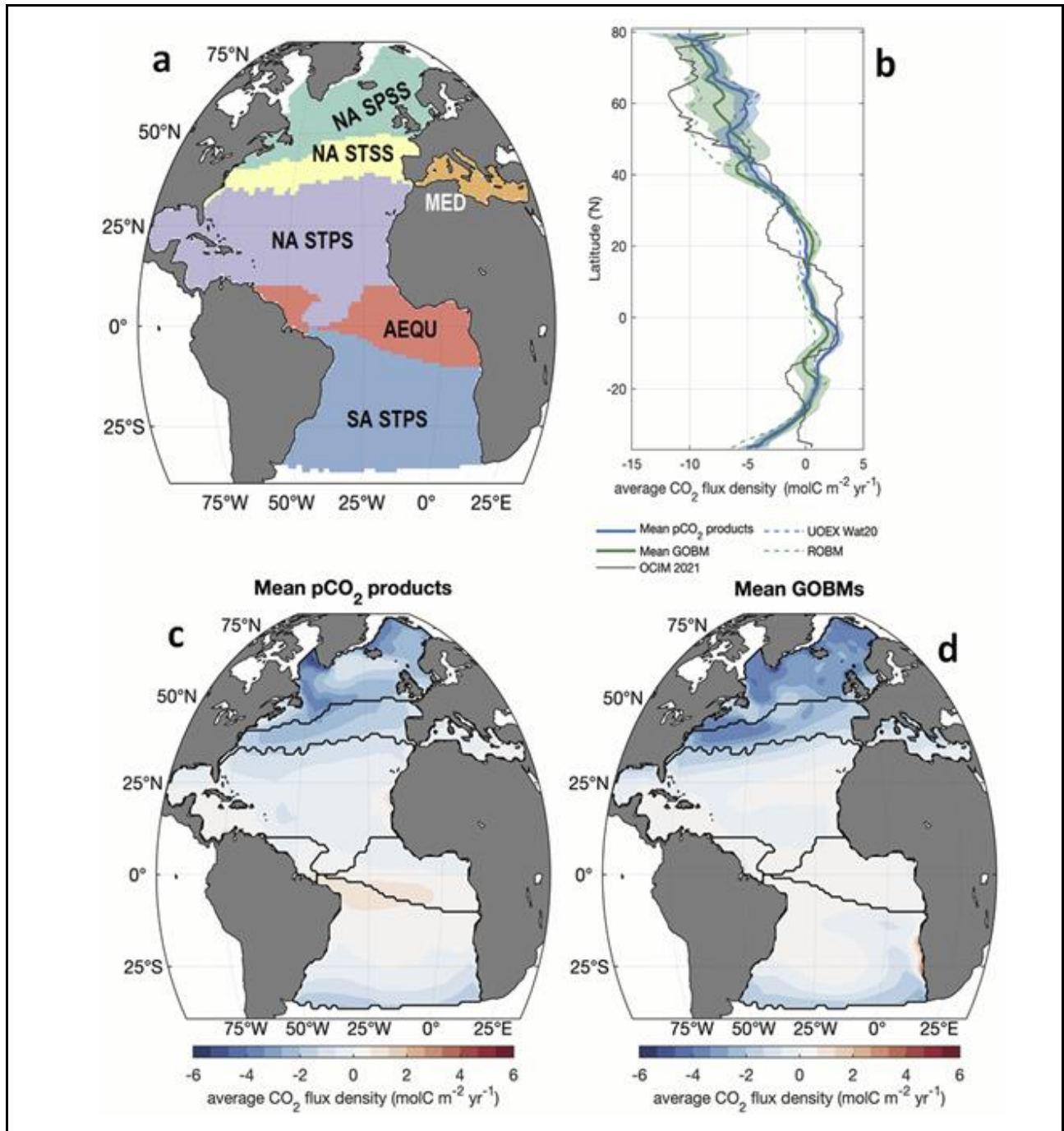


Figure 1. a) RECCAP2 biomes in the Atlantic including the Mediterranean Sea. b) Latitudinal variation of CO₂ flux densities displayed for the ensemble mean of the pCO₂ products, the GOBM ensemble mean, the UOEX data product that corrects for skin temperature effects, the regional hindcast model (ROBM), and the inverse model OCIMv2021. Average CO₂ flux density from 1985 to 2018, illustrated on maps for the ensemble means of c) nine pCO₂ products and d) eleven GOBMs. Negative values indicate oceanic uptake of CO₂. The biomes are the North Atlantic subpolar gyre seasonally stratified (NA SPSS), the seasonally and permanently

stratified regions of the North Atlantic subtropical gyre (NA STSS and NA STPS), the Atlantic equatorial upwelling region (AEQU), the seasonally stratified South Atlantic subtropical gyre (SA STPS), and the Mediterranean Sea (MED). Note that the GOBMs do not adequately represent the RCO fluxes and that we did not adjust those with other available estimates.

400 Integrated over the whole Atlantic Ocean, the average sea-air CO₂ flux (FCO₂) for the period
 401 1985 to 2018 obtained from the GOBMs (-0.47 ± 0.15 PgC yr⁻¹) is higher than that obtained from the
 402 pCO₂ products (-0.36 ± 0.06 PgC yr⁻¹; Figure 2), although the difference is within the FCO₂ variability
 403 across the 11 GOBMs. OCIMv2021 estimates a larger uptake (-0.58 ± 0.08 PgC yr⁻¹) than the
 404 GOBMs. The ROBM simulates an uptake of -0.61 ± 0.14 PgC yr⁻¹, about 30% and 65% stronger than
 405 the mean of the GOBMs and pCO₂ products, respectively. Relative to the mean of the pCO₂ products,
 406 the CO₂ uptake in UOEX is larger by about 23%.

407

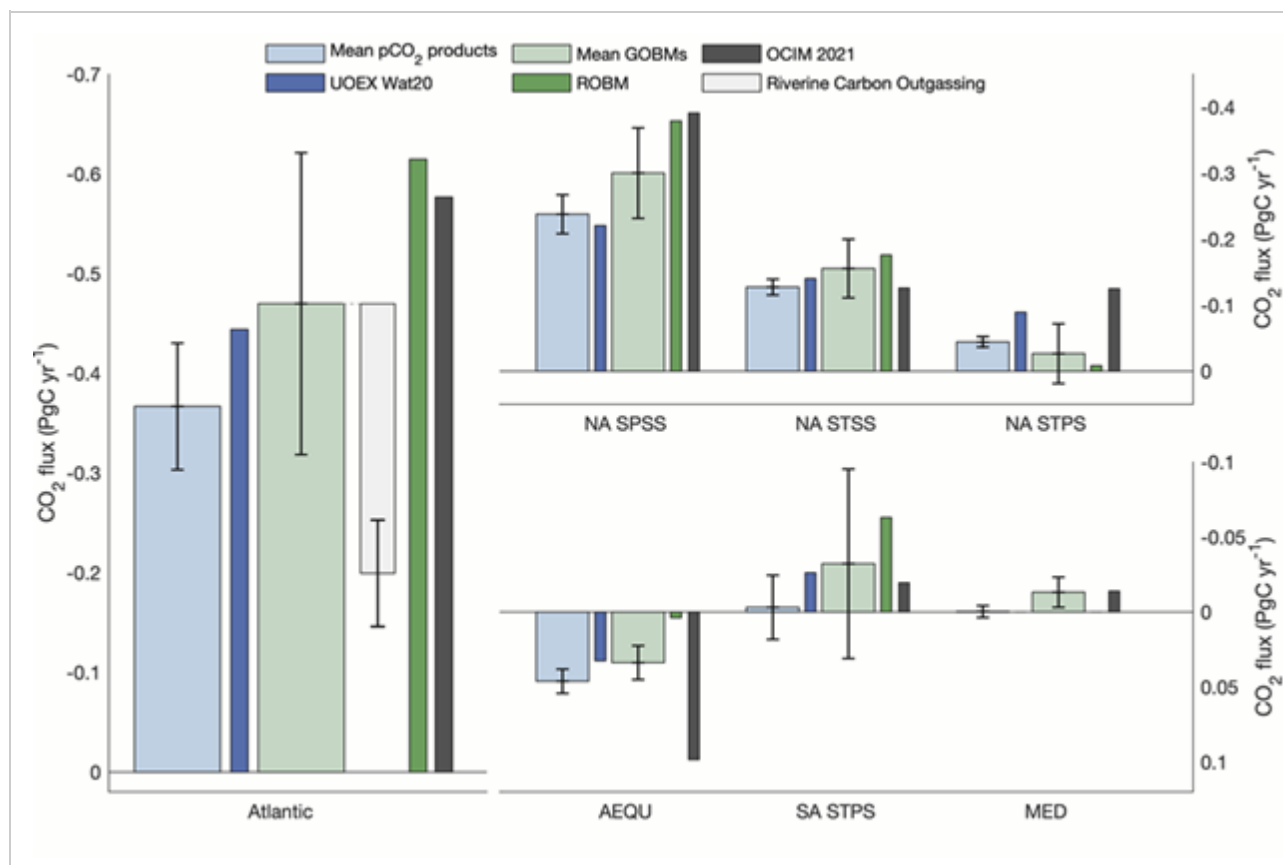


Figure 2. a) Spatially integrated sea-air CO₂ fluxes from 1985 to 2018 for the Atlantic and each Atlantic biome as estimated by nine pCO₂ products, ten GOBMS, the UOEX pCO₂-data product, the ROBM and OCIMv2021. The white bar indicates an estimate for the outgassing of riverine carbon integrated over the whole Atlantic region, which is a flux component captured by the pCO₂ products but not by the GOBMs or the ROBM. Whiskers stand for standard deviation around the mean of estimates. Negative values indicate uptake of CO₂ from the atmosphere. Note

that the y-axes are reversed, so that uptake is above the zero-line and outgassing is below it.

408 The NA SPSS biome, which covers only 15% of the Atlantic Ocean surface area, has the
 409 largest CO₂ uptake and also the largest differences between models and observational products
 410 (Figures 1 and 2, Table 1). Here, the mean FCO₂ of the GOBMs, the ROBM and OCIMv2021 indicate
 411 26, 59 and 64% greater carbon uptake, respectively, than the pCO₂ products. The spread between
 412 GOBMs is three times larger than it is for the pCO₂ products (Table S4). The uptake flux in UOEX
 413 is slightly lower (~7%) relative to the mean of pCO₂ products.

414 In the NA STSS biome, there is good agreement between the different pCO₂ products, with a
 415 standard deviation that is less than 10% of the mean (-0.13±0.01 PgC yr⁻¹). Here, the UOEX product
 416 has 10% larger CO₂ uptake. With an average FCO₂ of -0.15±0.04 PgC yr⁻¹, the GOBMs vary
 417 substantially more among each other, i.e., ±30%. In fact, one GOBM has a ~50% weaker uptake than
 418 the GOBMs mean, while the GOBMs with the most intense fluxes are only 20% above the GOBMs
 419 mean. OCIMv2021 simulates FCO₂ values of similar magnitude to the pCO₂ products (Table S4).

420 For the NA STPS biome, pCO₂ products estimate a mean CO₂ uptake of -0.044±0.008 PgC
 421 yr⁻¹ with a very high homogeneity in spite of the large area of this biome. In comparison to the pCO₂
 422 products, the uptake simulated by the GOBMs is smaller, (-0.020±0.040 PgC yr⁻¹), and with larger
 423 intermodel variations. Only three GOBMs estimated a CO₂ outgassing in this biome. In contrast,
 424 OCIMv2021 reported a quite high uptake of CO₂, almost three times larger than that of the pCO₂
 425 products. The ROBM simulates a near-zero net flux in this biome. In the UOEX product, the uptake
 426 is twice as large as the mean of the other pCO₂ products.

427 All models and pCO₂ products agree that the AEQU biome is a net source of CO₂ to the
 428 atmosphere, consistent with the known impact of the equatorial upwelling that brings water with high
 429 DIC content to the ocean surface. The mean flux of the pCO₂ products is 0.046±0.009 PgC yr⁻¹. In
 430 the UOEX product this outgassing is 25% lower. The mean flux in the GOBMs is 0.035±0.011 PgC
 431 yr⁻¹, and has relatively small inter-model variations. The ROBM simulates a very low outgassing.
 432 OCIMv2021 shows strong FCO₂, with more than double the outgassing of the mean GOBMs.

433 The SA STPS biome covers a large area, extending from the southern border of the equatorial
 434 region in the north towards the subtropical front of the Southern Ocean in the south. According to the
 435 mean of the pCO₂ products, the integrated flux over this region is neither a sink nor source of CO₂ to
 436 the atmosphere (-0.003±0.023 PgC yr⁻¹). But, the spread across the pCO₂ products is relatively large
 437 in this region, second only to the spread in the NA SPSS, in part because of the large area of the SA
 438 STPS biome. On average the GOBMs indicate that this region is a CO₂ sink with an estimated
 439 integrated flux of -0.029±0.076 PgC yr⁻¹. However, an integrated outgassing is simulated by 1/3 of
 440 the GOBMs. The FCO₂ in the ROBM is nearly twice as large as the mean of the GOBMs, while the
 441 OCIMv2021 suggested that the region behaves as a weaker CO₂ sink.

442 In the Mediterranean Sea, only five of the nine pCO₂ products have a regional coverage better
 443 than 95%. These four pCO₂ products agree that the biome does not present significant sea-air CO₂
 444 fluxes (Figure 2 and Table S4). Most of the GOBMs have a coverage better than 95% and they broadly

445 agree that the Mediterranean Sea represents a very weak CO₂ sink (-0.015 ± 0.010 PgC yr⁻¹). The flux
446 in the OCIMv2021 is very similar. The ROBM has insufficient regional coverage for an assessment
447 in this biome.

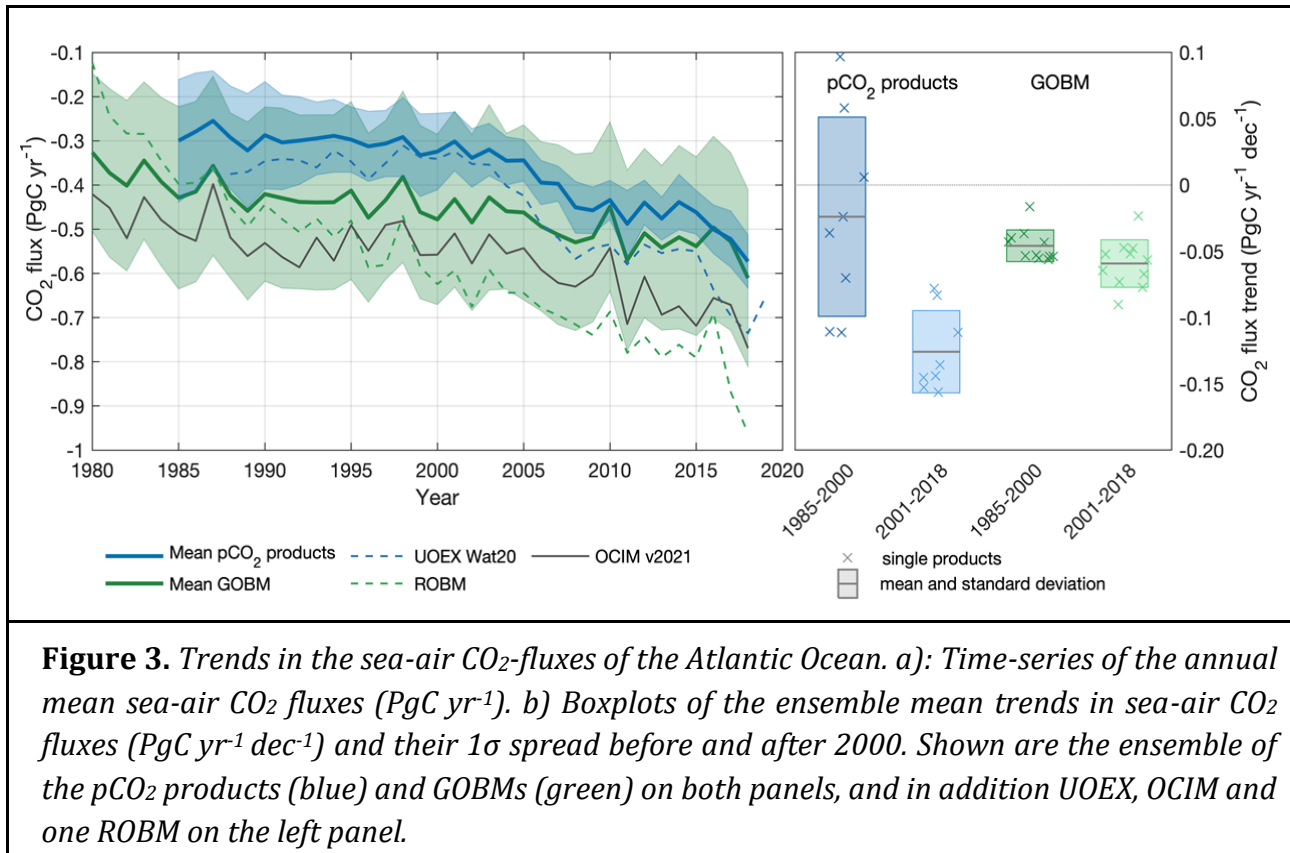
448 In summary, for the Atlantic, the GOBMs predict a $28\pm 14\%$ larger CO₂ uptake than pCO₂
449 products (Table 1). The regional and data-assimilation models simulate a stronger Atlantic CO₂ sink
450 than pCO₂ products by 67 and 57%, respectively (Table S4). The same is the case for the UOEX
451 product, where the CO₂ uptake is 25% larger than that of the mean pCO₂ products, as a consequence
452 of its adjustment for near surface temperature gradients.

453 3.1.2 FCO₂ trends

454 The temporal evolution of the annual mean sea air fluxes in the pCO₂ products shows a change
455 of rate around the year 2000 (Figure 3). In agreement with the recommended core analysis in
456 RECCAP2, we thus analyzed the changes in FCO₂ during two periods: between 1985 and 2000, and
457 between 2001 and 2018. Over these two periods, the atmospheric CO₂ concentration increased on
458 average by 1.5 and 2.1 ppm yr⁻¹, respectively, representing an acceleration in the atmospheric growth
459 rate of 43% from the first to the second period. Integrated over the Atlantic as a whole, the pCO₂
460 products indicate a 5-fold increase in the growth rate of the ocean carbon sink from -0.024 ± 0.075
461 PgC yr⁻¹ dec⁻¹ between 1985 and 2000 to -0.126 ± 0.031 PgC yr⁻¹ dec⁻¹ between 2001 and 2018 (Figure
462 3). In contrast, GOBMs simulate only a 33% increase in the growth rate between the two periods, i.e.,
463 from -0.045 ± 0.012 PgC yr⁻¹ dec⁻¹ between 1985 and 2000 to -0.060 ± 0.017 PgC yr⁻¹ dec⁻¹ between
464 2001 and 2018 (Figure 3). This is only slightly below the observed acceleration in the atmospheric
465 CO₂ growth rate. The two products differ also strongly with regard to their spreads (Figure 3b). While
466 the pCO₂ products exhibit a relatively low spread for the 1985-2018 mean flux, they differ
467 considerably with regard to their FCO₂ trends. Conversely, GOBMs show large spread in the 1985-
468 2018 mean flux, but have a low spread in their FCO₂ trends in both periods, reflecting that the trends
469 in the GOBMs are more strongly governed by the rate of change in atmospheric CO₂.

470 The CO₂ uptake trend increases in OCIMv2021 from -0.045 ± 0.016 PgC yr⁻¹ dec⁻¹ during the
471 first period to -0.111 ± 0.018 PgC yr⁻¹ dec⁻¹ for the second period. Its estimate is thus similar to that of
472 the GOBMs in the first period but almost twice as large in the second. The ROBM simulates a much
473 stronger growth than the GOBMs in both periods (-0.19 ± 0.02 and -0.14 ± 0.02 PgC yr⁻¹ dec⁻¹, but no
474 significant change in trend). On the other hand, the UOEX pCO₂ product reveals an even greater
475 contrast between the growth rates before 2000 (0.048 ± 0.014 PgC yr⁻¹ dec⁻¹) and after 2000 ($-$
476 0.188 ± 0.012 PgC yr⁻¹ dec⁻¹) than the ensemble mean of the pCO₂ products. The trends obtained by
477 the UOEX product showed a weakening of CO₂ uptake in the Atlantic Ocean before 2000, and an
478 increase of about 0.35 PgC yr⁻¹ in the second period, which is higher than in any of the other eight
479 pCO₂ products (range: 0.14 to 0.28 PgC yr⁻¹). Three of the other pCO₂ products also suggest a
480 weakening of the CO₂ uptake in the Atlantic before 2000, while four other products suggest increasing
481 trends in CO₂ uptake by the Atlantic. Possibly the sharp contrast in observational coverage before
482 and after the year 2000 (Figure S1; Bakker et al., 2022), as well as the availability of observed
483 predictor data affected in a noticeable way some of the products. Indeed, the agreement among pCO₂

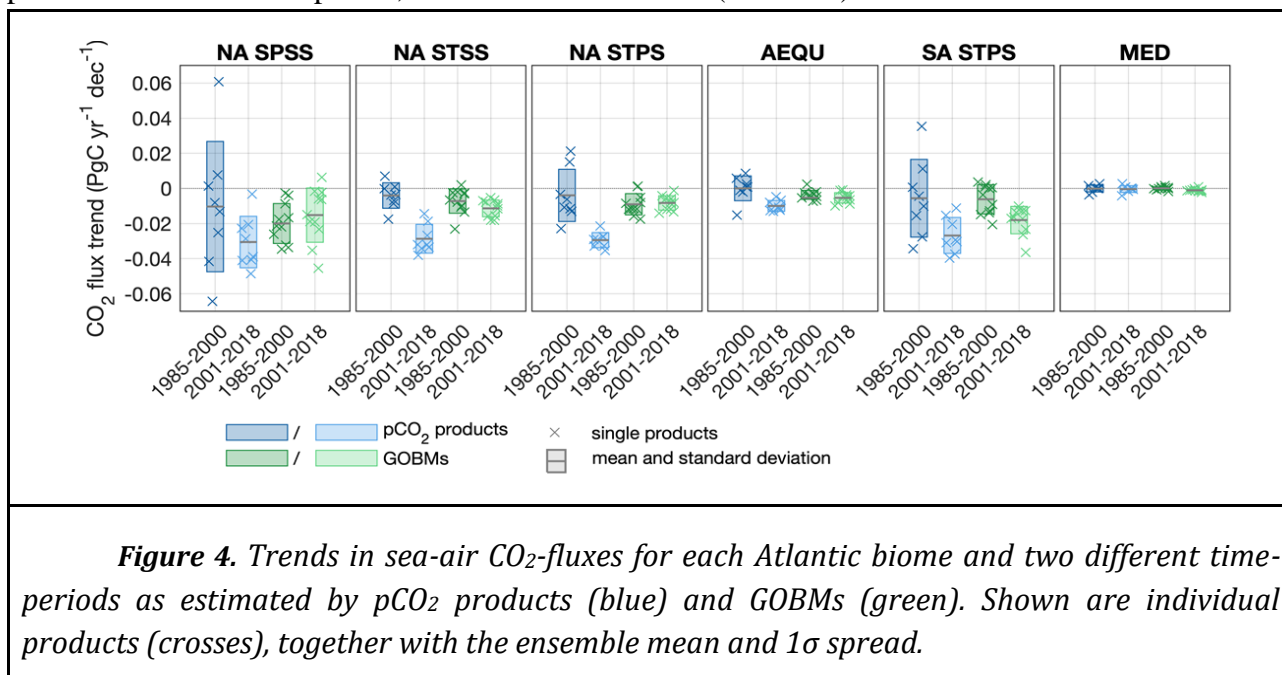
484 products significantly improved throughout the 1985-2000 period. This underscores a notable
 485 distinction from the GOBMs, as the observation-based trends in the initial period are markedly
 486 influenced by early-year FCO₂ estimates (refer to Figure S2). During this period, only limited pCO₂
 487 observations and predictor variables are available, and most products rely on climatologies of specific
 488 predictors, such as chlorophyll and mixed layer depth, due to a scarcity of observational data.



489
 490 Temporal trends in the individual biomes of the Atlantic are variable and highly dependent
 491 on the products used to estimate them (see Figure 4 and Table S5). Between 2001 and 2018, the pCO₂
 492 products show that the CO₂ uptake rate grows with values close to -0.03 PgC yr⁻¹ dec⁻¹ in the NA
 493 SSPS, NA STSS, NA STSS and SA STPS biomes (which present very different areas) and -0.01 PgC
 494 yr⁻¹ dec⁻¹ in the AEQU biome. During this period, all pCO₂ products agree on the sign of the trend in
 495 all biomes, with the exception of the MED biome where the trend was consistently close to zero.
 496 However, for the period 1985-2000, trends in CO₂ uptake estimated by the pCO₂ products are more
 497 variable across the different products and biomes, with non-significant trends in FCO₂ in NA STPS
 498 (-0.004±0.015 PgC yr⁻¹ dec⁻¹), AEQU (0.000±0.001 PgC yr⁻¹ dec⁻¹), and SA STPS (-0.006±0.022 PgC
 499 yr⁻¹ dec⁻¹) and mark a notable contrast between the two periods.

500 The biome-level trends are more consistent across the GOBMs than across the pCO₂ products,
 501 and also more similar in the two periods. In three biomes, NA STSS, AEQU and SA STSS, the
 502 GOBMs simulate on average an increase in fluxes to the ocean between the first and the second

503 period. The disagreement among the GOBMs and between GOBMs and pCO₂ products is largest in
 504 the NA SPSS biome. The ROBM shows rates of increase of CO₂ uptake higher than -0.03 PgC yr⁻¹
 505 dec⁻¹ in practically all biomes and in both periods except in NA STPS in the second one, and AEQU
 506 biomes in both (see Table S5). OCIMv2021 shows similar rates of increase to those observed in pCO₂
 507 products for the second period, in line with the ROBM (Table S5).

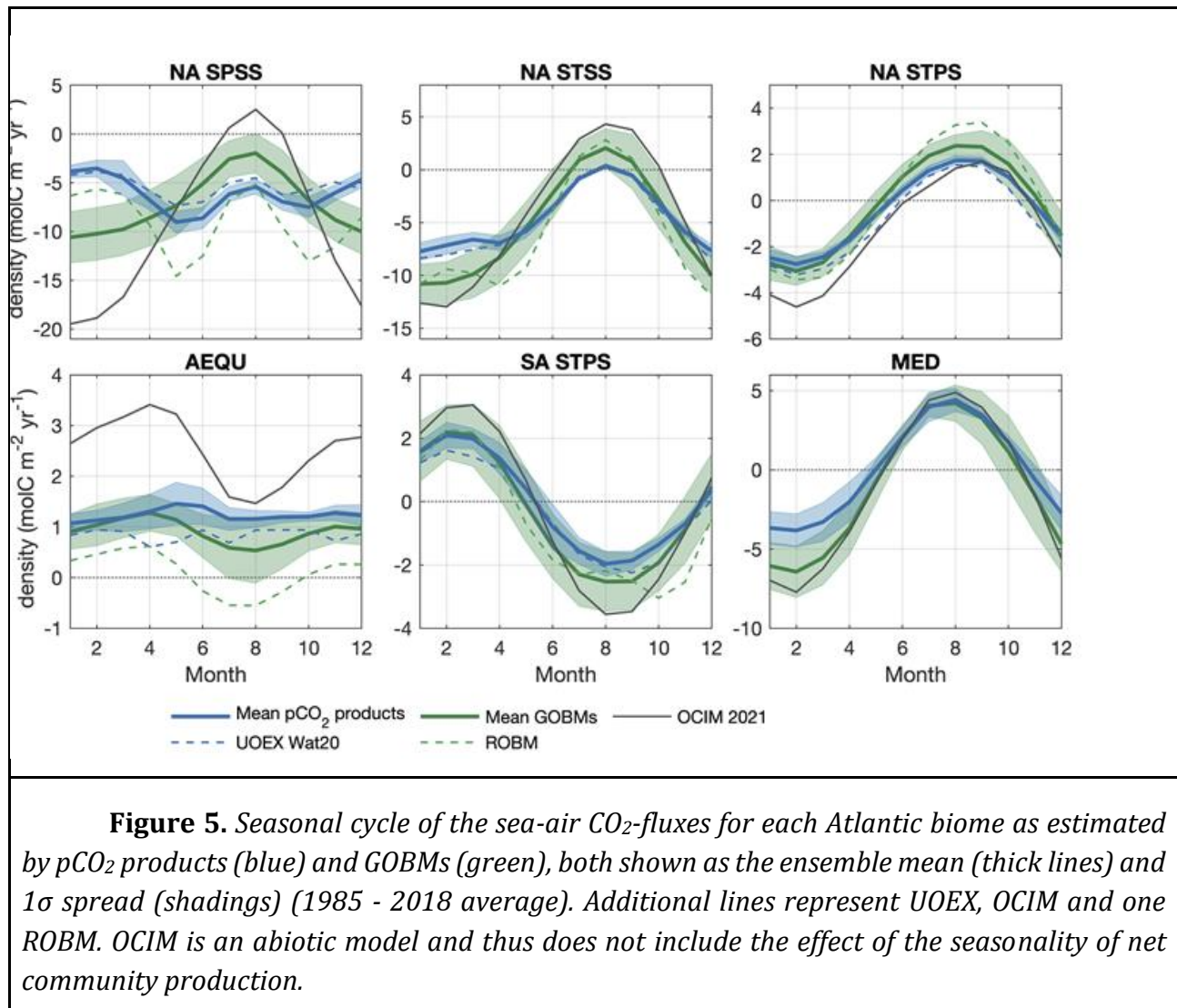


508

509 3.1.3 Seasonal cycle

510 The Atlantic Ocean sea-air CO₂ flux varies seasonally in a pronounced manner in all biomes,
 511 except for the equatorial (Figure 5). The Mediterranean Sea and the subtropical biomes (in their
 512 respective hemispheres) are CO₂ sinks in winter and sources in summer. Here, the impact of
 513 biological DIC drawdown on pCO₂ is relatively weak and seasonal warming and cooling dominates
 514 the seasonal cycle such that it peaks and reaches supersaturation in summer while minimum and
 515 undersaturated values occur in winter (Figure S3, S4 and Rodgers et al., 2023). The seasonal
 516 amplitude in the flux in these regions is slightly larger in the GOBMs than in the pCO₂ products. This
 517 has been attributed to a likely underestimation of seasonal mixed layer depth changes and seasonal
 518 drawdown of DIC by net primary production, such that the thermal component on the seasonal pCO₂
 519 and sea-air CO₂ flux cycle is too strong in these models (Rodgers et al., 2023). The OCIMv2021
 520 is an abiotic model and shows the largest seasonal pCO₂ (Figure S3) and flux variations because of the
 521 complete absence of biological processes. The difference in the seasonal cycle as modeled by the
 522 OCIMv2021 and the other GOBMs can be taken as a rough estimate of the importance of biology.

523



524

525 In the NA SPSS biome, the GOBMs' seasonal CO_2 flux cycle is similar to that in the
 526 subtropical biomes (and of the abiotic OCIM model), while that of the pCO_2 products is broadly
 527 reversed, apart from the summertime intermediate minimum in CO_2 uptake (Figure 5). The pCO_2
 528 products have the highest pCO_2 values in winter, as a consequence of the supply of remineralized
 529 DIC into the surface layer through deep mixing (Figure S3). Seasonal stratification and increased
 530 light availability triggers spring blooms that cause a sharp pCO_2 decrease from March to June, after
 531 which the pCO_2 steadily increases back to its winter maximum. The existence of these patterns is
 532 well known from the many direct observations in this region (Takahashi et al., 1993; Olsen et al.,
 533 2008; Fröb et al., 2019, Becker et al., 2018). The opposite seasonal pCO_2 cycle in the GOBMs is
 534 likely due to the fact that their seasonal variations in mixed layer depths are too small (Rodgers et al.,
 535 2023), such that too few nutrients are upwelled during winter, likely resulting in an underestimation
 536 of summer biological drawdown of DIC in the GOBMs (Rodgers et al., 2023; also shown for Earth

537 System Models in Goris et al., 2018). Since the opposing seasonal cycle of the GOBMs leads to a
538 lower pCO₂ at the time of the strongest wind speeds, the GOBM ensemble shows higher annual net
539 NA SPSS CO₂ uptake (Figures 1 and 2), i.e., the GOBMs tend to simulate too strong uptake. Again,
540 the OCIMv2021, as an abiotic model, is an extreme example of these model-effects. The ROBM
541 appears more consistent with the pCO₂ products in this regard, but it overall appears to overestimate
542 the NA SPSS CO₂ uptake as the modeled pCO₂ values are too low (Figure S3). The summertime
543 intermediate minimum in CO₂ uptake in the pCO₂ products is a consequence of the minimum in wind
544 speeds in that season. More quantitative analyses of the seasonal cycle including their drivers and
545 differences between GOBMs and pCO₂ products are presented by Rodgers et al. (2023).

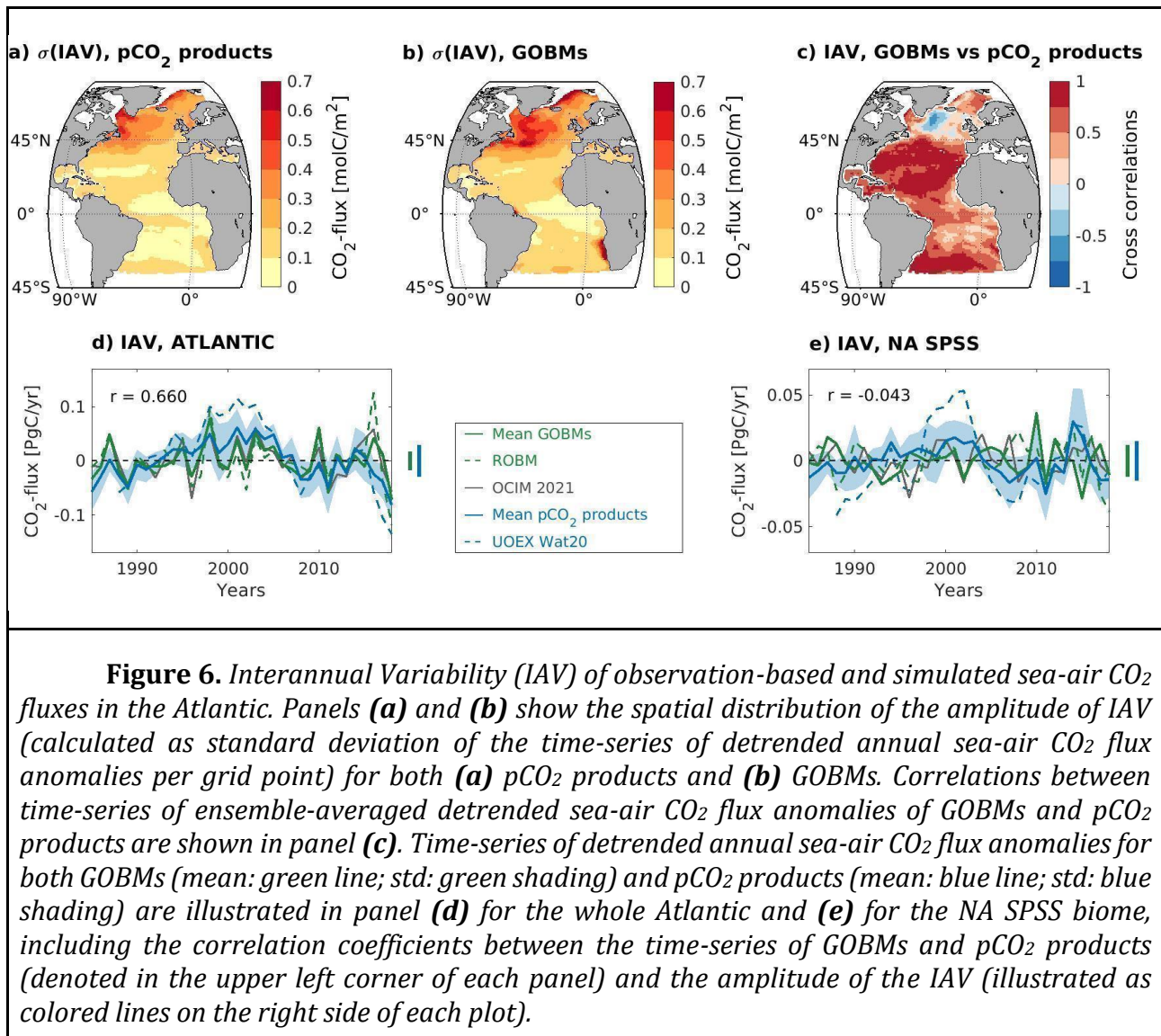
546

547 3.1.4 Interannual Variability of the sea-air CO₂ fluxes

548 We further analyzed the interannual variability (IAV) of sea-air CO₂ fluxes, determined as the
549 annual anomaly of the detrended sea-air CO₂ fluxes with respect to their mean values. Here, the
550 removed linear trends and means are considered over the period 1985-2018 for pCO₂ products and
551 GOBMs. When referencing the amplitude of IAV, we refer to the standard deviation of the so-derived
552 detrended sea-air CO₂ flux anomalies. We find that, over the whole Atlantic basin, the IAV time-
553 series of the sea-air CO₂ fluxes of GOBMs and pCO₂ products correlate relatively well (Figure 6d).
554 Furthermore, both pCO₂ products and GOBMs show a high IAV amplitude in the northern parts and
555 low IAV amplitude in the equatorial region (Figure 6a,b). This general spatial pattern of the IAV
556 amplitude of net sea-air CO₂ fluxes has also been found in other studies (Brady et al., 2019; Park et
557 al., 2010). Yet, the GOBMs show a larger IAV amplitude than the pCO₂ products in the interior
558 subpolar gyre as well as in the eastern boundary upwelling regions (Figure 6a,b), while showing a
559 smaller IAV amplitude for the NA SPSS biome as a whole (Figure 6e).

560 The pCO₂ products and GOBMs agree on the phasing of the IAV in net sea-air CO₂ fluxes,
561 apart from in the subpolar region where correlations are small and negative (Figure 6c, e; Figure S5).
562 We note that there is also little agreement in the IAV of this biome between pCO₂ products (Figure
563 S6), while the GOBMs agree relatively well (Figure S6). GOBMs and pCO₂ products agree that the
564 total sea-air CO₂ fluxes of the biomes NA STSS, NA STPS and SA STPS are characterized by a
565 moderate IAV amplitude (Figure S7), and that biomes AEQU and MED have only a weak IAV
566 amplitude (see Figure S5). For these five biomes, GOBMs and pCO₂ products correlate reasonably
567 well with respect to the temporal variability of the IAV with correlation coefficients ranging from
568 $r=0.57$ to $r=0.73$ (see also Figure S5).

569



570

571 For the GOBM ensemble, the IAV of net sea-air CO_2 fluxes is strongly positively correlated
 572 to the IAV in SST (higher FCO_2 in anomalously warm years) over large parts of the Atlantic basin;
 573 most notably for both permanently stratified biomes (SA STPS and NA STPS) and the northwestern
 574 subpolar gyre (Figure S8b). Along the Gulf Stream and the North Atlantic Current as well as regions
 575 of equatorial upwelling, the IAV in net sea-air CO_2 fluxes of the GOBM ensemble is weakly
 576 negatively correlated to the IAV in SST (higher FCO_2 in anomalously cold years). Due to the known
 577 dynamics of net sea-air CO_2 fluxes, these negative correlations imply that SST-variations are not the
 578 main driver of the IAV in net sea-air CO_2 fluxes but that the anomalous cold years are likely
 579 accompanied by stronger mixing and hence more DIC upwelling. As the thermodynamic boundary
 580 conditions used to force the GOBMs result in SSTs that have relatively strong fidelity to observations
 581 when averaged over biome scales, it is plausible that the relatively small model spread around the

582 IAV in the Atlantic is related to the fact that most of the simulated IAV is driven by SST-variations
583 (areas with positive correlations in Figure S8b) and that variations in DIC play a less important role.
584 The strong relationship to SST is also the plausible cause for high correlations between IAV in net
585 sea-air CO₂ fluxes of pCO₂ products and GOBMs in SA STPS and NA STPS. Indeed, when
586 correlating the IAV in net sea-air CO₂ fluxes of pCO₂ products to the IAV in SST (Figure S8a), we
587 find strong correlations in SA STPS and NA STPS biomes. However, in the NA SPSS, the pCO₂
588 products appear to be more negatively correlated to the IAV in SST (likely driven by DIC variations),
589 in contrast to the GOBMs. This difference in mechanisms over the subpolar gyre is one possible
590 explanation for the disagreement in the IAV in net sea-air CO₂ fluxes between pCO₂ products and
591 GOBMs in the NA SPSS biome.

592 In the North Atlantic, one of the most prominent climate variability modes at interannual time
593 scales is the NAO. In a study about the influences of NAO on the IAV of North Atlantic CO₂ fluxes,
594 Jing et al. (2019) noted that, in summer, SST is important for the IAV in pCO₂ in the subtropical
595 North Atlantic, while biogeochemical variables probably control the pCO₂ IAV in the subpolar North
596 Atlantic. When relating the IAV of the GOBMs to NAO, we find significant but weak correlations
597 for the NA SPSS and the AEQU biomes ($r=-0.43$, $p=0.01$ and $r=-0.48$, $p=0.004$), whereas all other
598 biomes show no significant correlation to the NAO index. Yet, the pCO₂ products show a similar
599 correlation between NAO and IAV for the AEQU biome ($r=-0.41$, $p=0.02$), but no significant
600 correlation in the NA SPSS biome (neither for the average nor for single products). The similar
601 correlation in the AEQU is consistent with the fact that in this region, temperature-driven Atlantic
602 Niño climatic mode plays an important role in modulating the IAV of CO₂ fluxes (Koseki et al.,
603 2023), and that the GOBMs simulated SST variability is well constrained by the observations. The
604 absent correlation in the NA SPSS could be due to the opposing imprints of NAO on pCO₂ in the
605 western and eastern domains of the NA SPSS. In a modeling study, Tjiputra et al. (2012)
606 demonstrated that during positive NAO, SST cooling induces a negative pCO₂ anomaly in the western
607 subpolar gyre, whereas in the eastern part (in the proximity of the Irminger Sea) anomalously deep
608 winter mixing upwells DIC-rich water masses and induces a positive pCO₂ anomaly (e.g., Fröb et al.,
609 2019). The opposite mechanism is suggested during negative NAO.

610 We note that despite relatively high correlations between IAV of GOBMs and pCO₂ products
611 in all biomes apart from the NA SPSS (Figure 6c), the amplitude of the IAV of the GOBMs is smaller
612 than that of pCO₂ products in all biomes except the NA STSS (Figure S5). The amplitude of the IAV
613 of the total sea-air CO₂ fluxes in the Atlantic basin is 0.029 ± 0.01 PgC yr⁻¹ (pCO₂ products) and
614 0.018 ± 0.005 PgC yr⁻¹ (GOBMs). These results are significantly different but of similar magnitude
615 as the linear trends of the sea-air CO₂ fluxes of the Atlantic basin (Figure 3). For a better estimate of
616 the sea-air CO₂ fluxes in the Atlantic basin, it is hence important to have an accurate estimate of both
617 temporal variability and amplitude of the IAV, which is currently not adequately represented.
618 Moreover, the temporal disagreement of IAV of pCO₂ products in the NA SPSS makes it clear that a
619 closer examination of the gap filling methods and their dynamic realism is urgently needed here
620 (Hauck et al., 2023, Gloege et al., 2021).

621 3.2 Ocean interior C_{ant} accumulation from 1994-2007

622 The change in the oceanic storage of anthropogenic carbon (ΔC_{ant}) was evaluated for the period 1994-
 623 2007 for comparison between GOBMs, the data-assimilation model OCIMv2021 and two
 624 observation-based ΔC_{ant} reconstruction products. All nine considered GOBMs simulated an increase
 625 in the basin-wide C_{ant} inventory that is broadly consistent among themselves and with observations
 626 (Table S6). Seven models show high column inventory changes of C_{ant} in the NA SPSS biome and in
 627 the NA STSS, consistent with the observation-based ΔC_{ant} reconstructions (Fig. S9), while the other
 628 two (PlankTOM12 and CESM-ETHZ) show high ΔC_{ant} column inventories in the vicinity of 35°S,
 629 but very weak accumulation in the North Atlantic.

630
 631 **Table 1.** Sea-air surface CO_2 fluxes (1985-2018) and anthropogenic CO_2 accumulation rates (1994-
 632 2007) of all products used in this study, with their respective standard deviations. For ΔC_{ant} the MED
 633 biome is not included in the total Atlantic estimate to facilitate direct comparison with Gruber et al.
 634 (2019). In each biome, the graduate yellow color background sorts the estimates from lowest flux
 635 into the ocean (light yellow) to largest flux into the ocean (dark yellow), as well as the estimates from
 636 lowest ΔC_{ant} (light yellow) to largest ΔC_{ant} (dark yellow).

		FCO_2 [PgC yr^{-1}]			
Period	BIOME (Area · 10^{12})	pCO_2 products <i>Ensemble mean</i>	GOBM <i>Ensemble mean</i>	ROBM <i>ROMS-ETHZ</i>	Assimilation model <i>OCIMv2021</i>
1985-2018	ATLANTIC (68.7)	-0.37 ± 0.06	-0.47 ± 0.15	-0.61 ± 0.15	-0.58 ± 0.08
	NA SPSS (9.37)	-0.24 ± 0.03	-0.30 ± 0.07	-0.38 ± 0.05	-0.40 ± 0.03
	NA STSS (6.14)	-0.127 ± 0.012	-0.149 ± 0.041	-0.176 ± 0.022	-0.126 ± 0.012
	NA STPS (22.7)	-0.044 ± 0.008	-0.020 ± 0.041	-0.008 ± 0.026	-0.125 ± 0.024
	AEQU (8.69)	0.046 ± 0.008	0.035 ± 0.011	0.004 ± 0.016	0.098 ± 0.005
	SA STPS (19.6)	-0.003 ± 0.021	-0.029 ± 0.065	-0.063 ± 0.040	-0.020 ± 0.022
	Med (2.26)	0.000 ± 0.005	-0.015 ± 0.009	-	-0.014 ± 0.003
		ΔC_{ant} [PgC yr^{-1}]			
Period	BIOME (Area · 10^{12})	C_{ant} reconstruction <i>Gruber et al., 2019</i>	C_{ant} reconstruction <i>Khatiwala et al., 2009</i>	GOBM <i>Ensemble mean</i>	Assimilation model <i>OCIMv2021</i>
1994-2007	ATLANTIC (68.7)	0.72 ± 0.08	0.63 ± 0.11	0.52 ± 0.11	0.68 ± 0.01
	NA SPSS (9.37)	0.087 ± 0.007	0.149 ± 0.027	0.087 ± 0.033	0.127 ± 0.001
	NA STSS (6.14)	0.098 ± 0.005	0.105 ± 0.018	0.080 ± 0.031	0.107 ± 0.001
	NA STPS (22.7)	0.254 ± 0.017	0.199 ± 0.036	0.175 ± 0.045	0.236 ± 0.002
	AEQU (8.69)	0.058 ± 0.018	0.040 ± 0.007	0.037 ± 0.006	0.054 ± 0.001
	SA STPS (19.6)	0.216 ± 0.041	0.137 ± 0.007	0.127 ± 0.018	0.156 ± 0.001
	Med (2.26)	-	-	0.0176 ± 0.0068	0.0186 ± 0.0001

637

638 The spatial distribution of the change in column-integrated ΔC_{ant} averaged across the
639 ensemble of nine GOBMs is shown in Figure 7b. Spatial patterns in the ΔC_{ant} column inventory
640 distribution obtained by the OCIMv2021 inverse-model (Figure 7c) are very similar to the GOBM
641 ensemble mean but with higher values throughout the Atlantic, except in the region of the Brazil
642 Current and in the vicinity of the Azores Islands. In addition, OCIMv2021 produces a similar pattern
643 to that obtained from the DIC-based product from Gruber et al. (2019) (Figure 7a), but with stronger
644 (weaker) ΔC_{ant} in the northernmost regions (south of the equator). The GOBM ensemble mean reveals
645 slightly higher ΔC_{ant} column inventories in the subpolar North Atlantic than the observation-based
646 product from Gruber et al. (2019) (Figure 7d). In contrast, over the tropical and South Atlantic, the
647 ΔC_{ant} column inventory of the GOBM ensemble is only about half as high as the reconstruction of
648 Gruber et al. (2019), representing the main discrepancy between both products.

649 Integrated over the whole Atlantic Ocean, the ΔC_{ant} inventory simulated by the GOBM
650 ensemble (Table 1) is about $28 \pm 20\%$ lower than the inventory estimate obtained with the observation-
651 based eMLR(C*) method (Gruber et al., 2019), 17% lower than the age-tracer based method
652 (Khatiwala et al., 2009), and $28 \pm 15\%$ lower than the inverse model OCIMv2021. By contrast, the
653 OCIMv2021 ΔC_{ant} inventory is very similar to the estimate from Gruber et al. (2019), while 8% higher
654 compared to that of Khatiwala et al. (2009).

655 Integrated over the individual biomes of the Atlantic, we found the best agreement between
656 the GOBM ensemble and the estimate from Gruber et al. (2019) in the northern biomes. In the NA
657 SPSS and NA STSS biomes, C_{ant} accumulation rates are very similar between GOBMs, and only two
658 models show extraordinarily low values (50% lower than the GOBMs average; Table S6). In contrast,
659 OCIMv2021 simulates a ΔC_{ant} inventory that is about 40% higher than the observation-based estimate
660 and the GOBM ensemble mean, and therefore closer to the values obtained with the Green's Function
661 (Khatiwala et al., 2009). Further south, discrepancies between the GOBM-based and the observation-
662 based ΔC_{ant} inventories increase, bringing the GOBM inventories closer to the age-tracer based
663 product, while OCIMv2021 resembles the eMLR(C*)-based estimates in two of the three remaining
664 biomes. In the NA STPS biome, characterized by the largest inter-GOBM spread, the ΔC_{ant} inventory
665 of the GOBMs is about 25% lower than the observation-based product, while the OCIMv2021
666 inventory reveals a similar rate of change as the observation-based product. Likewise, in the AEQU
667 biome, the GOBMs' ensemble mean ΔC_{ant} inventory is approximately 30% lower than that from
668 Gruber et al. (2019) and OCIMv2021. The AEQU biome further reveals the lowest ΔC_{ant} inventories
669 with a very narrow inter-GOBMs spread. The largest ΔC_{ant} inventory difference between the GOBMs
670 and the observation-based product exists in the SA STPS biome, with a GOBM ΔC_{ant} storage rate
671 nearly 50% lower than that of Gruber et al. (2019). In addition, in the SA STPS biome, the
672 OCIMv2021 ΔC_{ant} inventory is also 30% lower than that of Gruber et al. (2019). No comparison is
673 done for the MED biome because of the lack of data in ΔC_{ant} reconstruction products.

674

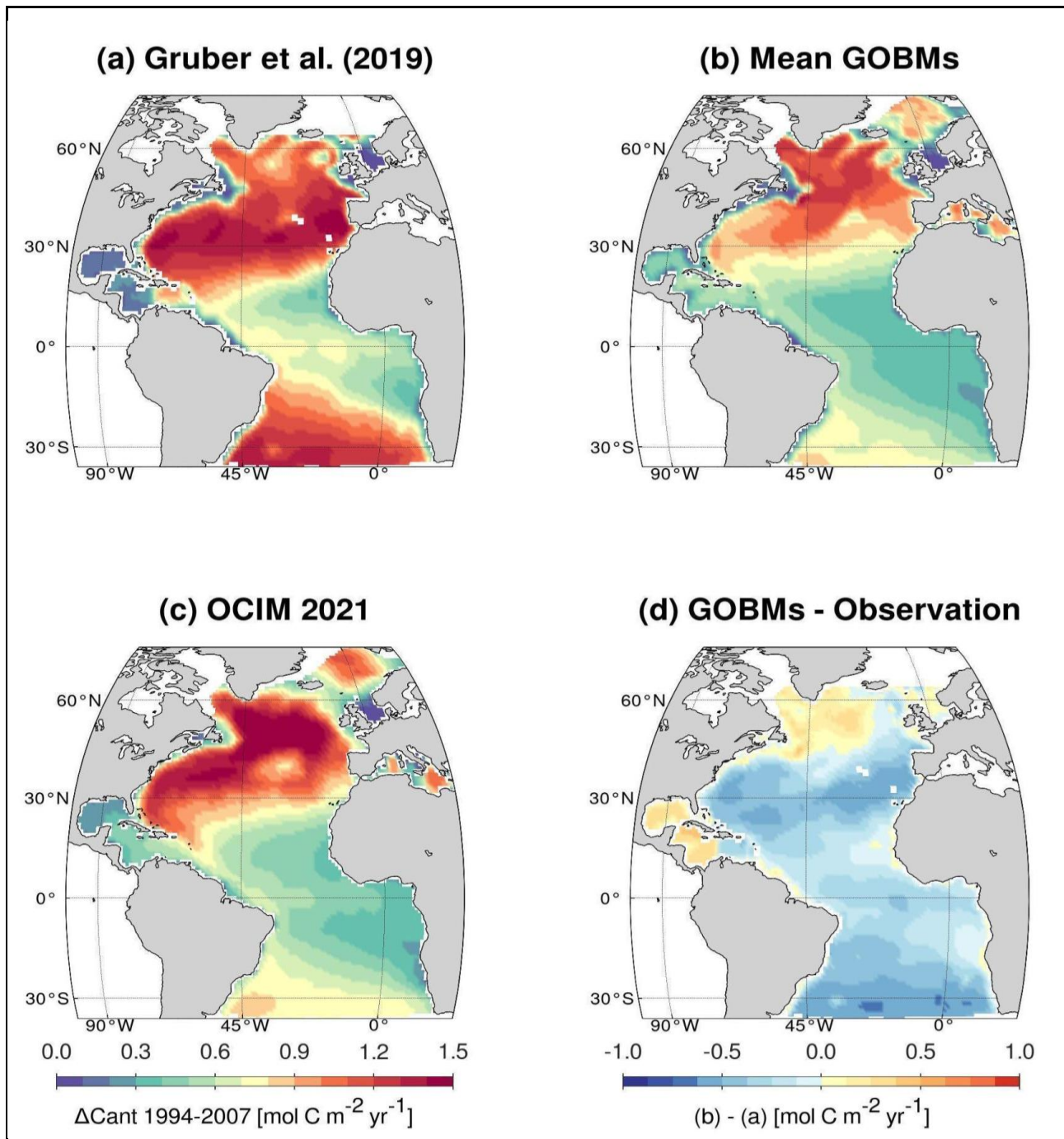


Figure 7. Column inventories of anthropogenic carbon storage changes (ΔC_{ant}), integrated from surface to 3000 m from 1994 to 2007. Shown are ΔC_{ant} column inventories for **a)** an observation-based reconstruction with the eMLR(C^*) method by Gruber et al. (2019); **b)** multi-model GOBM ensemble mean **c)** OCIMv2021. Panel **d)** illustrates the difference between the estimates from GOBM ensemble mean and Gruber et al. (2019).

675

676 Average ΔC_{ant} vertical profiles of each biome and for the whole Atlantic (Figure S10) reveal

677 that the maximum ΔC_{ant} occurs near the surface, while the accumulation rates decrease rapidly with
 678 depth. In general, GOBMs simulations and the estimates from Gruber et al. (2019) agree with regard
 679 to this vertical distribution, both in the Atlantic and at biome-level. However, in the NA STPS, AEQU
 680 and SA STPS biomes, the observation-based reconstruction presents a second ΔC_{ant} maximum
 681 between 1400 and 3000 m depths that is only reproduced by the GOBMs in the NA STPS. Such depth
 682 range is associated with waters with moderate values of C_{ant} transported by the DWBC circulating
 683 southward below the Antarctic Intermediate Water ΔC_{ant} minimum (Rhein et al. 2015; Fajar et al.
 684 2015; Rios et al. 2012; Rios et al. 2003), mainly North Atlantic Deep Water (NADW). That the
 685 GOBMs do not agree with the observations in the southernmost biomes (AEQU and SA STPS) could
 686 be indicative of how the GOBMs ventilate the ocean interior below 1400 m during 1994 - 2007 period.
 687 Updated reconstructions with the eMLR(C*) method by Müller et al. (2023) detect these deep-water
 688 accumulations only for the period from 1994 to 2004 but not from 2004 to 2014. These findings could
 689 either indicate that (i) ΔC_{ant} in the NADW is subject to larger decadal scale variability than simulated
 690 in GOBMs, that (ii) the observational data from the 1990s used for the reconstructions from Gruber
 691 et al. (2019) as well as the first decade of the reconstruction by Müller et al. (2023) contribute to
 692 unidentified biases in the observation-based estimates, or that (iii) the statistical gap-filling with the
 693 eMLR method approaches its limits in reconstructing the low C_{ant} accumulation rates in these water
 694 masses.

695 3.3 Anthropogenic CO₂ uptake and lateral transport

696 In terms of recent storage changes in C_{ant} , GOBMs tend to simulate lower accumulation rates
 697 than observation-based estimates (Section 3.2), whereas we have previously described that the net
 698 CO₂ uptake is larger in GOBMs than pCO₂ products (Section 3.1.1). To assess this apparent
 699 inconsistency, the anthropogenic component of the CO₂ fluxes in GOBMs is assessed from the
 700 differences of Simulation A minus Simulation D in each GOBM, allowing us to determine the sea-
 701 air fluxes caused solely by increased CO₂ in the atmosphere. The anthropogenic FCO₂ averaged
 702 across 9 GOBMs (F_{ant}) in the Atlantic as a whole is shown in Figure 8 and for each of the biomes in
 703 Figure S11. Integrated over the whole Atlantic, the F_{ant} fluxes are lower in magnitude than the net
 704 flux FCO₂ because the natural flux component contributes an additional CO₂ uptake in the NA SPSS
 705 and NA STSS biomes. In the other biomes the natural contributions are lower or even represent
 706 positive fluxes (outgassing) (Figure S11). However, the net result for the Atlantic Ocean is an uptake
 707 of natural CO₂ (approx $\sim 0.1 \text{ PgC yr}^{-1}$ obtained from the Simulation B) being transported to the
 708 Southern Ocean. In terms of C_{ant} , the biome with the highest uptake is also the NA SPSS, although
 709 the latitudinal variability is by far not as marked as in the natural component of FCO₂.

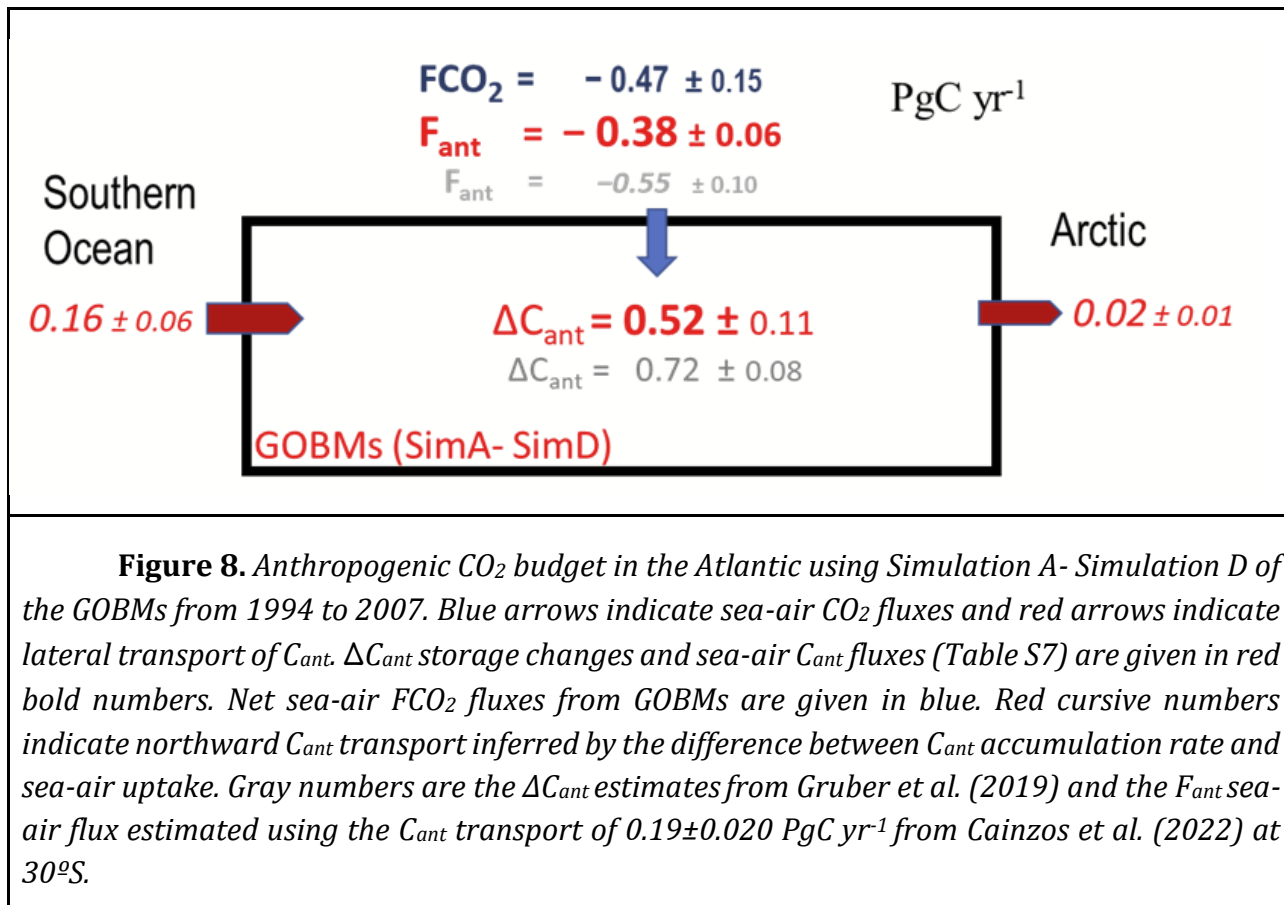
710 Knowing the C_{ant} accumulation rate in the ocean interior and the flux entering from the
 711 atmosphere, we can infer horizontal transport rates (Figures 8 and S11). Given the enclosed
 712 bathymetry of the Mediterranean Sea, the GOBM ensemble simulates a mean net export of C_{ant} from
 713 the Atlantic to the Mediterranean of $0.0055 \pm 0.0050 \text{ PgC yr}^{-1}$, inferred as the residual between an
 714 accumulation rate of $0.018 \text{ PgC yr}^{-1}$ and C_{ant} uptake from the atmosphere at a rate of $-0.012 \text{ PgC yr}^{-1}$
 715 (Figure S11). This inferred C_{ant} import to the Mediterranean Sea is consistent with the observation-

716 based transport estimates in the Strait of Gibraltar of $0.0042 \pm 0.0010 \text{ PgC yr}^{-1}$ (Huertas et al., 2009).

717 From estimates of the exchange between the Nordic Seas and the Arctic (Jeansson et al., 2011)
718 and the exchange from the Nares Strait, a net flux to the Arctic of $0.02 \pm 0.01 \text{ PgC yr}^{-1}$ was estimated.
719 With this, the remaining lateral transport rates between the different biomes were estimated for each
720 GOBM as the difference between surface flux, interior accumulation and the boundary fluxes. From
721 the average of the GOBM results (lateral C_{ant} transport and F_{ant} , Figure S11), the average transport
722 from the Southern Ocean is obtained (Figure 8).

723 For the Atlantic, the northward transport of C_{ant} from the Southern Ocean decreases northward
724 to almost zero (Figure S11) or reverses sign at the boundary between the NA STSS and NA SPSS
725 biomes. These C_{ant} transports are fully compatible with the AMOC, in which the upper branch
726 transports more C_{ant} northward than the southward lower branch, and also with the decrease of the
727 vertical gradient of C_{ant} northward such that in the NA SPSS biome the vertical gradient of C_{ant} is
728 small (Figure S10). With these results, the net transports of $0.163 \pm 0.057 \text{ PgC yr}^{-1}$ at the South
729 Atlantic boundary obtained from the GOBM results are consistent with recent transports estimated
730 from ocean sections at 30°S of $0.186 \pm 0.019 \text{ PgC yr}^{-1}$ (Cainzos et al., 2022). This suggests that the
731 weak anthropogenic sea-air CO_2 fluxes are the primary cause of low ΔC_{ant} in the South Atlantic. The
732 lower ΔC_{ant} in the interior ocean and in particular in the NA STPS and SA STPS biomes suggest that
733 the anthropogenic contribution to the total FCO_2 in GOBMs is 30% weaker than expected from C_{ant}
734 observations in the interior ocean. Although the total FCO_2 obtained from GOBMs are stronger in the
735 Atlantic than those derived from pCO_2 products, we note that the total FCO_2 from the GOBMs contain
736 no RCO correction here. While our estimate of the anthropogenic contribution is unaffected by RCO,
737 this is not true for the FCO_2 estimates of the GOBMs. If we were to apply the RCO-values based on
738 Regnier and Lacroix et al. (2020) to the FCO_2 estimates of the GOBMs, then their total FCO_2 estimate
739 would be weaker than that derived by the pCO_2 products.

740 The inferred northward C_{ant} transport at the southern boundary between Atlantic and Southern
741 Oceans obtained for each of the nine GOBMs with Simulations A and D shows a high correlation
742 ($r^2=0.61$; $p\text{-level}<0.01$) with the maximum AMOC values at 26°N of each of these GOBMs (Figure
743 S12), indicating that the northward physical transport is the main driver of the northward C_{ant}
744 transport. We note additionally that, in comparison with observations, the GOBMs tend to
745 underestimate the maximum AMOC values at 26°N (Figure S12) and hence the inferred northward
746 C_{ant} transport (Terhaar et al., 2024).



747

748 **4. Discussion**749 *4.1 Progress since RECCAP1*

750 Over the last decade, the nature of the pCO_2 products has changed significantly, not only
 751 because of a significant growth in the number of observations (Bakker et al., 2016) but also because
 752 of the implementation of new data interpolation methodologies (e.g., Rödenbeck et al., 2015, Denvil-
 753 Sommer et al., 2019; Gregor et al., 2019), and improvements in the fidelity of predictor variables.
 754 This led to RECCAP2 being able to use nine different pCO_2 products with time-varying FCO_2
 755 estimates. RECCAP1 only had 2 products available for time-varying Atlantic Ocean FCO_2 estimates:
 756 a multi-parameter regression based on the gridded product of SOCATv1.5 (Pfeil et al., 2012) as well
 757 as regional scale FCO_2 estimates based on the pCO_2 database analysis of McKinley et al. (2011).
 758 Additionally, the climatology of Takahashi et al. (2009) formed a cornerstone of the RECCAP1
 759 studies and has proven to be a very robust product, with estimates close to the climatologies obtained
 760 from the new pCO_2 products. On the modeling side, there have also been many relevant advances
 761 between RECCAP1 and RECCAP2. In RECCAP1, only six models were used while RECCAP2
 762 employs almost twice the number of models. A subset of the available GOBMs in RECCAP2 also
 763 participated in RECCAP1 and have been improved in both physical and biological processes (e.g.,
 764 Aumont et al., 2015; Schwinger et al., 2016; Wright et al., 2021), with an enhanced spatial resolution

765 (e.g., from $\sim 2^\circ$ to $\sim 1^\circ$), though they remain too coarse to resolve mesoscale processes.

766 A direct comparison between RECCAP1 and RECCAP2 estimates of the Atlantic cannot be
767 performed due to the appreciable improvements in methods and data coverage. Moreover, the
768 estimates made in RECCAP1 have a different regional domain (spanning from 44°S to 79°N). The
769 zonal region from 35°S to 44°S is no longer part of the Atlantic Ocean mask in RECCAP2, but instead
770 considered to be part of the Southern Ocean (Hauck et al., 2023). In addition, the time period covered
771 in RECCAP1 spans the years 1990 to 2009, while RECCAP2 covers the years from 1985 to 2018 and
772 considers not only the whole time-period but also two sub-periods (before and after 2000). In
773 RECCAP1, an estimate of RCO flux component ($0.17 \pm 0.04 \text{ PgC yr}^{-1}$) was subtracted from the FCO_2
774 values obtained for GOBMs (see Table S8 for details), which was not performed here. However, to
775 allow a direct comparison with RECCAP1 (Table S8), we additionally calculated FCO_2 averages for
776 the region from 44°S to 79°N for the RECCAP1 time period. To compare the GOBM estimates, we
777 additionally re-added the RCO-flux to the RECCAP1 estimate. Our inferred RECCAP2-results for
778 the FCO_2 averages are similar to those published in RECCAP1 (Schuster et al., 2013) as the FCO_2
779 estimates are within the uncertainty of each other (Table S8). Yet, the mean FCO_2 -values increased
780 in both the GOBM ensemble mean (21% increase) and pCO_2 product ensemble average (9%
781 increase). Both the RECCAP1 as well as the RECCAP2 estimate show a higher average FCO_2 -value
782 for the GOBMs, yet the mean difference between GOBMs and pCO_2 products is larger in RECCAP2.

783 It is difficult to compare estimates of decadal trends between RECCAP1 and RECCAP2, as
784 RECCAP1 only provided upper-bound estimates for the trends based on the pCO_2 -database. The
785 GOBMs of RECCAP1 estimated the largest trends in FCO_2 for the North Subtropics and estimated
786 the trends for the other Atlantic regions to be negligible or very small (Schuster et al., 2013). We
787 cannot confirm this in RECCAP2 (Figure 4) because our trend estimates consider different time-
788 periods and that the IAV could additionally influence the trend-estimates substantially (e.g., Figure
789 4).

790 For the IAV in FCO_2 , Schuster et al. (2013) found in RECCAP1 significant but weak
791 correlations to the NAO for the Equatorial biome with opposing signs between GOBMs ($r=-0.43$) and
792 pCO_2 products ($r=0.35$), potentially relating to their IAV being driven by SST-variations and DIC-
793 variations, respectively. Here, the new definition of the Equatorial biome in RECCAP2 helps to
794 confine the upwelling region such that the IAV in this region is DIC driven in both GOBMs and pCO_2
795 products, with correlations of $r=-0.40$ and $r=-0.47$ with the NAO, respectively. In our case, negative
796 correlations indicate DIC-driven variations as we correlate the NAO with the sea-to-air flux, while
797 Schuster et al. (2013) correlated it with the air-to-sea flux (i.e. flux of opposite sign). Yet, the issue
798 of the GOBMs being more SST-driven remains also within the IAV of RECCAP2; most notably in
799 the North Atlantic subpolar gyre.

800 In terms of FCO_2 seasonality, the southern subtropical regions, the equatorial region and
801 northern subtropics studied in RECCAP1 followed the seasonal increase and decrease of pCO_2 driven
802 mainly by warming and cooling in both GOBMs and observation-based estimates. These general
803 results remain consistent in our analysis.-In the NA SPSS, the RECCAP1 pCO_2 products showed that

804 the seasonal cycle is reversed with a minimum during summer and outgassing in winter (Schuster et
 805 al., 2013), conforming to direct observations (Olsen et al., 2008) whereas the seasonal cycle of
 806 GOBMs was dominated by the temperature component. As the Atlantic regions in RECCAP1 were
 807 defined simply via latitudinal boundaries, Schuster et al. (2013) denoted that the temperature
 808 controlled seasonal cycle of the GOBMs is likely due to the inclusion of the northern reaches of the
 809 subtropical gyre. The refinement of the Atlantic regions in RECCAP2, however, shows that
 810 biogeochemical boundaries with a clearer exclusion of the subtropical gyre do not change the
 811 temperature control of the seasonal cycle of the GOBMs in the NA SPSS.

812 Even though RECCAP2 benefits from a substantial increase in observations and
 813 improvements in modeling (complexity and resolution), the mean difference between GOBMs and
 814 pCO₂ products is larger in RECCAP2 and the disagreements between pCO₂ products and GOBMs in
 815 the NA SPSS remain in terms of IAV and seasonal cycle. Potential mechanisms for this are further
 816 discussed in Section 4.3.

817 *4.2 The influence of the riverine CO₂ outgassing on comparisons of the CO₂ sink in RECCAP2* 818 *models and observation-based products*

819 When averaged over the 1985 to 2018 period, the mean FCO₂ of pCO₂ products and GOBM
 820 ensemble agree within the ranges of their ensemble spread for most of the biomes and the Atlantic
 821 basin (Table 1). The related spatial distribution of FCO₂ also agrees with respect to the large-scale,
 822 basin-wide patterns (Figure 1), although some discrepancies are detected in the NA SPSS biome. The
 823 average Atlantic FCO₂ estimated by the GOBM ensemble is 30% lower than the estimate from pCO₂
 824 products.

825 The riverine carbon outgassing (RCO, see Methods 2.4) hampers the comparison of the FCO₂
 826 estimates from the GOBMs with those of pCO₂ products, since the input of riverine carbon and the
 827 burial of carbon is treated in various ways across the ensemble of GOBMs. Furthermore, relevant
 828 output from the GOBMs is missing to properly assess the contribution of carbon, alkalinity and
 829 nutrient input from land and their burial in sediments, resulting in a situation where only a rough
 830 approximation of the RCO in the GOBMs is possible (Terhaar et al., 2024). In the RECCAP2
 831 protocol, it was recommended to apply the spatial distribution of the RCO of Lacroix et al. (2020),
 832 scaled to a globally integrated RCO value of $0.65 \pm 0.3 \text{ PgC yr}^{-1}$ (Regnier et al., 2022). This procedure
 833 results in a large adjustment of $0.27 \pm 0.06 \text{ PgC yr}^{-1}$ ($3.9 \pm 1.0 \text{ mol C m}^{-2} \text{ yr}^{-1}$) for the Atlantic sea-air
 834 CO₂ flux, which is more than half of the FCO₂ derived from the set of GOBMs and 70% of that
 835 estimated from pCO₂ products (in absolute numbers). Although other estimates of the RCO reported
 836 by Aumont et al. (2001) and Jacobson et al. (2007) reduce the RCO in the Atlantic by 1/3, the relative
 837 magnitude of the RCO compared to the FCO₂ from GOBMs and pCO₂ products remains substantial.

838 In the Atlantic Ocean the difference between the FCO₂ obtained by the ensemble pCO₂
 839 products and the ensemble of GOBMs is $0.10 \pm 0.11 \text{ PgC yr}^{-1}$. The RCO derived from Aumont et al.
 840 (2001), Jacobson et al. (2007), and Lacroix et al. (2020) scaled up to Regnier et al. (2022) are
 841 0.16 ± 0.05 , 0.16 ± 0.04 , and $0.27 \pm 0.06 \text{ PgC yr}^{-1}$, respectively (Table S3), yielding an ensemble average
 842 of $0.20 \pm 0.05 \text{ PgC yr}^{-1}$. All four of these values are higher than the average difference between the

843 pCO₂ products and GOBMs, although within the combined uncertainty of all estimates. Importantly,
 844 for four of the five biomes (NA SPSS, NA STSS, AEQU and SA STPS), the ensemble RCO-estimates
 845 agree well with the FCO₂ differences (pCO₂ products minus GOBMs) with a mean difference of only
 846 -0.001 ± 0.019 PgC yr⁻¹ when the ensemble of RCO is added to the GOBMs estimate (last column in
 847 Table S3).

848 The biome with the largest discrepancy between FCO₂ in the GOBMs and in the pCO₂
 849 products is the NA STPS. Likewise, the three estimates of the RCO diverge most in this biome,
 850 indicating a high RCO-uncertainty. The FCO₂ difference between pCO₂ products and GOBMs would
 851 require an RCO of -0.024 ± 0.013 PgC yr⁻¹ to be balanced, i.e., an additional CO₂ uptake rather than
 852 outgassing due to riverine input of carbon. However, this difference is of reversed sign and much
 853 lower than the ensemble mean of the direct RCO estimates ($+0.073 \pm 0.048$ PgC yr⁻¹, Table S3). This
 854 discrepancy would be even larger when the RCO estimate recommended in RECCAP2
 855 ($+0.126 \pm 0.010$ PgC yr⁻¹) would be used. At the same time, the ΔC_{ant} (Table 1) and F_{ant} rates of the
 856 GOBMs in the NA STPS biome are lower than an observation-based estimate from Zunino et al.
 857 (2015), who used DIC measurements along the 26.5°N and 7.5°N sections from 1992/93 and 2010/11,
 858 and inferred a F_{ant} of -0.23 ± 0.02 PgC yr⁻¹ over an area of $15.3 \cdot 10^{12}$ m² (70% of NA STPS), which is
 859 more than twice the estimated F_{ant} in the GOBMs (-0.084 ± 0.010 PgC yr⁻¹, Figure S11). The F_{ant}
 860 difference between the GOBMs and the observation-based estimate from Zunino et al. (2015) is very
 861 similar to the difference between the direct RCO estimate ($+0.126 \pm 0.040$ PgC yr⁻¹) and the residual
 862 between the FCO₂ from pCO₂ products and GOBMs (-0.024 ± 0.013 PgC yr⁻¹). This agreement in the
 863 differences suggests that the GOBMs indeed underestimate the C_{ant} uptake in the NA STPS biome. If
 864 the GOBMs simulated a substantially stronger C_{ant} uptake (by about -0.1 PgC yr⁻¹), then the direct
 865 RCO estimate would plausibly explain the FCO₂ difference between the GOBMs and pCO₂ products,
 866 albeit with large uncertainty. The likely underestimation of F_{ant} by the GOBMs in the NA STPS biome
 867 is further supported by their ΔC_{ant} that is only about half as large as the observation-based estimate
 868 from Gruber et al. 2019 (Table 1), as well as the lower northward C_{ant} transport compared to two
 869 observation-based estimates (Brown et al. 2021; Cainzos et al. 2022).

870

871 *4.3 Temporal variability in sea-air CO₂ fluxes in models and pCO₂ products*

872 In the results section, differences between models and pCO₂ products in sea-air CO₂-flux dynamics
 873 are described in terms of trends, seasonality and interannual variability. The region where the GOBMs
 874 and pCO₂ products show the largest discrepancies is the NA SPSS: the biome with the highest CO₂
 875 uptake rates. When looking at the seasonal decomposition of surface pCO₂, it becomes clear that the
 876 seasonality is primarily temperature-driven in the GOBMs so that their CO₂ uptake is larger in winter
 877 than in summer because of the seasonal SST changes. The seasonal cycle of the pCO₂ products is
 878 driven by DIC variations (for more information see Figure S4 and Rodgers et al., 2023). In the North
 879 Atlantic subpolar gyre, direct observations of interannual variability in winter pCO₂ have shown that
 880 this is associated with variations in mixed layer depths in this season (Fröb et al., 2019). That means
 881 that more intense mixing during colder winters leads to higher surface DIC and consequently higher

882 pCO₂, and thus a reduced flux of CO₂ into the ocean. A DIC-driven dynamic is supported by the
883 seasonal cycle of the pCO₂ products and the strong, negative correlation of the pCO₂ product between
884 the IAV of CO₂ flux and SST in this region (Figure S8a). On the other hand, the GOBMs simulate
885 positive correlations between IAV of CO₂ flux and SST. Hence the disagreement between pCO₂
886 products and GOBMs in IAV and seasonal cycle is interconnected and driven by the same cause:
887 SST-driven temporal variations in the GOBMs versus DIC-driven temporal variations in the pCO₂
888 products. We note that the NA SPSS is also the region in which pCO₂ products and GOBMs have the
889 largest disagreement in their mean CO₂-fluxes and the largest uncertainty in their CO₂-trends (see
890 Figures 1 and 4).

891 When looking for the underlying causes for the disagreement in seasonal driving forces and
892 IAV between pCO₂ products and GOBMs in the NA SPSS, we find that most of the GOBMs for
893 which the simulated AMOC is available show significant correlations between their IAV of CO₂
894 fluxes in the NA SPSS and AMOC-variations with correlation between 0.37 and 0.62. Further, using
895 Earth System Models, Goris et al. (2023) showed that the AMOC-strength drives the simulated
896 seasonal variability in the North Atlantic. Altogether, this suggests that the underestimation of the
897 AMOC in the GOBMs (Terhaar et al., 2024) could be an underlying cause for the underestimation of
898 the role of biogeochemical variability for both IAV and seasonality by the GOBMs in the NA SPSS.

899 Furthermore, we identify that the comparatively small DIC variations (as seen in both seasonal
900 cycle and IAV) in the GOBMs might also be a consequence of their current simplified set-up, or the
901 total lack, of riverine carbon fluxes (Terhaar et al., 2024). According to Aumont et al. (2001) and Gao
902 et al. (2023), the contribution of RCO weakens the CO₂ uptake in the NA subpolar gyre and in the
903 Southern Ocean. In fact, applying the predicted riverine carbon outgassing of Aumont et al. (2001)
904 to the NA SPSS biome removes the difference in FCO₂ mean fluxes (1985-2018) between pCO₂
905 products and GOBMs (Table S3). The RCO modeled by Aumont et al. (2001) also shows a similarity
906 (in numbers) to the mean FCO₂ differences (1985-2018) between GOBMs and pCO₂ products in the
907 NA STSS, AEQU and SA STPS biomes (Table S3). The study of Aumont et al. (2001) highlights the
908 importance of the slow reactivity of dissolved organic carbon (DOC) supplied by rivers to the regional
909 distribution of CO₂-fluxes, which hence might also be contributing significantly to seasonal and
910 interannual variability.

911 Finally, the different strengths of drivers and the resulting large disagreements in IAV between
912 GOBMs and pCO₂ products may leave an imprint on the calculated trends of the sea-air CO₂-fluxes
913 of the NA SPSS biome for the period 2001-2018 (Figure 4). Here, the pCO₂ products show an
914 accelerated trend for the period 2001-2018 which is not simulated by the GOBMs. Similarly, the IAV
915 of the pCO₂ products is in a positive phase in the year 2000 and in a negative phase in the year 2018
916 in the NA SPSS (Figure 6), which is not the case for the GOBMs. While this behavior is especially
917 pronounced in the NA SPSS, the NA STPS biome shows a similar phasing in their IAV when
918 comparing GOBMS and pCO₂ products. In a previous study (McKinley et al., 2020) it has been found
919 that the IAV is a potential driver of differences in trends between observational products and GOBMs.

920 While the IAV has an influence on the decadal trends, it cannot solely explain that the

921 calculated trends of sea-air CO₂ fluxes before and after the year 2000 are similar across our ensemble
922 of GOBMs, while the trends obtained from surface CO₂ observations show a sharp increase between
923 the trend of the pre-2000 and post-2000. We advise caution when comparing the CO₂ trends before
924 the year 2000 between GOBMs and pCO₂ products, as the trends of the pCO₂ products are strongly
925 conditioned by the FCO₂ estimates in the early years (Figure S2), where the available observations
926 (pCO₂ data and predictors) to generate the pCO₂ products are far less, such that the estimates of the
927 pCO₂ products agree less than in later years (Figures 3 and S2). In fact, the pCO₂ products do not
928 agree on the CO₂ trends before the year 2000 (-0.024 ± 0.075 PgC-yr⁻¹ dec⁻¹) with three pCO₂ products
929 suggesting a weakening of the CO₂ uptake in the Atlantic before 2000 and four pCO₂ products a
930 strengthening (Table S5). For the trends after the year 2000, the agreement of the pCO₂ products
931 allows for a more confident estimate of a strengthening CO₂ sink in the Atlantic with a trend of -
932 0.126 ± 0.031 PgC-yr⁻¹ dec⁻¹, which is twice the trend estimated by the GOBMs, of -0.060 ± 0.017 PgC-
933 yr⁻¹ dec⁻¹. Nevertheless, by using one of the pCO₂ products (MPI-SOM-FFN) in a model, it has been
934 shown that a bias in sampling locations influences the trends and an optimal sampling strategy reduces
935 the negative trend estimate in the northern hemisphere for the years 2000-2018 (Hauck et al., 2023).
936 Hence, a skewed sampling strategy could potentially influence the 2000-2018 trend estimate of the
937 pCO₂ products. For the GOBMs, we want to note that their simulated seasonal cycle might lead to a
938 trend estimate that is too low, as it has been shown for an ensemble of Earth System Models that a
939 more SST-driven seasonal cycle is related to shallower MLD and a less vivid AMOC (Goris et al.,
940 2018; 2023). Earth System Models with a weaker AMOC simulate more warming and less future
941 carbon uptake in the North Atlantic. Contrarily, a biology-driven seasonal cycle will lead to enhanced
942 carbon uptake due to the increasing sensitivity of pCO₂ to DIC variations with declining buffer
943 capacity of the ocean (Hauck et al., 2015).

944

945 *4.4 C_{ant} Storage and transport*

946 In the Atlantic, the GOBM ensemble C_{ant} accumulation rate (1994-2007) is $28 \pm 20\%$ lower
947 than the observation-based estimate of Gruber et al. (2019). In general, both GOBMs and the Gruber
948 et al. (2019) product show maximum C_{ant} concentrations near the surface with a rapid decrease
949 towards depth. Nevertheless, surface GOBM estimates are in general slightly lower than the
950 observation-based product, which might be related to biases in the Revelle factor caused by too high
951 preindustrial CO₂ values in a couple of GOBMs with a late starting date past 1765 (Terhaar et al.,
952 2024). The highest agreement between GOBMs and the observation-based product in ΔC_{ant} is found
953 north of 30°N, while the GOBMs simulate systematically lower accumulation rates in the South
954 Atlantic (Figure 7, Table 1). In the upper ocean layer, where the upper limb of the AMOC is located,
955 the differences in ΔC_{ant} are not particularly evident (Fig. S10). However, between 1400 and 3000 m
956 depths, GOBMs do not reproduce the C_{ant} peak estimated by the observation-based product (Rhein et
957 al. 2015; Rios et al. 2012; Fajar et al. 2015; Gruber et al. 2019) for the Atlantic (Figure S10) and,
958 more specifically, for the AEQU and SA STPS biomes. This depth interval, with lower ΔC_{ant} in
959 GOBMs compared to the observation-based estimate, coincides with the depth at which the NADW

960 is located. This result suggests that over the 1994-2007 period the GOBMs simulated too little C_{ant}
961 advection into the South Atlantic within the Deep Western Boundary Current that carries the C_{ant} -
962 rich NADW towards the Southern Hemisphere (Goris et al., 2023). This interpretation would be
963 consistent with the fact that most of the RECCAP2 GOBMs simulate too weak AMOC strengths
964 (Terhaar et al., 2024). In addition, we note that biased low C_{ant} uptake in the Southern Ocean (Hauck
965 et al., 2023), and the subsequent northward transport to the Atlantic, could also contribute to the too-
966 low ΔC_{ant} in the South Atlantic by GOBMs. However, the transport of C_{ant} from the Southern Ocean
967 to the Atlantic is in accordance with the observations (Cainzos et al., 2022). We also note that the
968 GOBMs may underestimate the temporal variability of the ocean interior transport, since the ΔC_{ant} of
969 the GOBMs in the South Atlantic are more similar to the estimates by Khatiwala et al. (2009), which
970 assumes a quasi-stationary ocean circulation (see Table 1 for SA STPS biome). In contrast, the
971 GOBMs show a lower decadal variability of the ΔC_{ant} than observation-based products (Gruber et al.
972 2019; Müller et al., 2023). The interannual variability of the ΔC_{ant} , derived from the linear regressions,
973 is typically $1.5 \pm 1.0\%$ of the absolute rates across all biomes and the whole Atlantic Ocean, indicating
974 that the ΔC_{ant} in the GOBMs occurs as a rather steady process.

975 The assessment of C_{ant} accumulation and transport in the Atlantic conducted in RECCAP1
976 (Khatiwala et al., 2013) revealed that the largest anthropogenic CO_2 uptake occurs in the Southern
977 Ocean, with much of this uptake being transported equatorward through the Antarctic Intermediate
978 Water and Subantarctic Mode Water. Most of this C_{ant} is stored in the SA STPS (Mikaloff Fletcher
979 et al., 2006). There is also a significant C_{ant} uptake in the tropical Atlantic that is partially transported
980 southward, but most of it is stored in the tropics or transported northward. The C_{ant} taken up in the
981 North Atlantic is transported northward in the upper limb of the AMOC and subsequently entrained
982 to the NADW and transported southward in the lower limb of AMOC. The GOBMs analyzed here
983 confirm these spatial patterns of ΔC_{ant} (though accumulation is low in the South Atlantic below 1500
984 m, Figures 7, S9, and S10) and of meridional transport (dominated by inflow from the Southern
985 Ocean, Figures 8 and S11).

986 Khatiwala et al., (2013) stated that the C_{ant} transports estimated from GO-SHIP sections using
987 hydrographic data and observation-based C_{ant} estimates (Holfort et al., 1998; Álvarez et al., 2003;
988 Macdonald et al., 2003; Rosón et al., 2003; Pérez et al., 2013) represent C_{ant} transport at a single time
989 point. Such C_{ant} transport estimates may be biased because seasonal variability is not resolved (Wilkin
990 et al., 1995). However, recent estimates cover long time series (Brown et al., 2021), or aim to provide
991 decadal climatological estimates (Cainzos et al., 2022). In RECCAP1, Khatiwala et al. (2013) showed
992 that C_{ant} transports, obtained based on GOBMs and from hydrographic sections, exhibit similar C_{ant}
993 transports between 44°S and the Equator with a northward transport of 0.15 to 0.20 PgC yr^{-1} , but, in
994 contrast, in the North Atlantic the GOBMs simulated a gradual northward decrease of the C_{ant}
995 transport, reaching zero horizontal net transport between 35° and 60°N . This pattern is confirmed in
996 RECCAP2 (Figure S11) with a larger number of GOBMs involved. Estimates of C_{ant} transport in the
997 26°N along transoceanic sections (Macdonald et al., 2003; Rosón et al., 2003; Perez et al., 2013;
998 Zunino et al. 2015; Brown et al, 2021; Cainzos et al., 2022) showed larger values than those of the
999 oceanic inversion or GOBMs. These discrepancies remained uncertain in RECCAP1 due to the

1000 uncertainties in the hydrographic estimates and the difficulties in directly comparing the two
1001 techniques. However, one must also consider the difficulties that inverse models and GOBMs have
1002 in representing mesoscale processes, mainly in regions of very intense currents such as the Florida
1003 Current, Gulf Stream, and DWBC (Khaliwala et al. 2013, Hirschi et al. 2020; Ma et al., 2016; Bower
1004 et al. 2019).

1005 Recent estimates by Brown et al. (2021) using the RAPID long time series (2004-2012), with
1006 an assessment of C_{ant} transports at 10-day timescale, confirm a strong C_{ant} transport at 26.5°N of
1007 $0.191 \pm 0.013 \text{ PgC yr}^{-1}$, which is in the middle of the range (0.128 ± 0.032 to $0.25 \pm 0.05 \text{ PgC yr}^{-1}$) of the
1008 eight estimates obtained from five sections between 1992 and 2011 (collected in Cainzos et al., 2022).
1009 The ensemble average C_{ant} transport over 26°N obtained for the nine GOBMs used here is
1010 $0.053 \pm 0.037 \text{ PgC yr}^{-1}$, which is almost four times lower than the C_{ant} transport of Brown et al. (2021).
1011 Racapé et al. (2018), using a global NEMO-PISCES model with a finer spatial resolution ($0.5^\circ \times 0.5^\circ$),
1012 obtained a northward transport of $0.092 \pm 0.04 \text{ PgC yr}^{-1}$ somewhat closer to observation-based
1013 estimates, suggesting that the spatial resolution of the GOBMs is relevant for the simulation of ocean
1014 interior transport. Observational-based evaluations of C_{ant} transport indicate the dynamical difficulties
1015 that CMIP5/6 climate models in certain regions have in achieving realistic projections of the AMOC
1016 and DWBC, when run at relatively coarse resolutions on the order of 1° (Hirschi et al., 2020; Ma et
1017 al., 2016), which does not allow to correctly simulate vertical structures nor to resolve mesoscale
1018 ocean eddies (Bower et al., 2019). For the RECCAP2 GOBMs, it was shown that the AMOC is, on
1019 average, underestimated by $3.1 \pm 5.2 \text{ Sv}$ at 26.5°N, which can partly explain this discrepancy between
1020 GOBMs and observation-based estimates (Terhaar et al., 2024).

1021 The weak C_{ant} northward transport in the subtropical region as shown by GOBMs might also
1022 be connected to a possible mismatch in C_{ant} uptake in the NA STPS biomes (Zunino et al., 2015)
1023 described above. Despite the agreement in mean FCO_2 between pCO_2 products and GOBMs in the
1024 NA STPS, the mismatch between the potentially strong RCO (Table S3) and the ‘residual RCO’
1025 (difference between GOBMs and pCO_2 products) further supports that the GOBMs simulate a too
1026 low C_{ant} uptake (Table S3) despite the apparent agreement in the net flux. The reduced C_{ant} uptake
1027 would be conveyed both northward and downward to the ocean interior. In fact, Cainzos et al. (2022)
1028 show that the contribution of vertical mixing is somewhat larger than the southward horizontal
1029 advection of ΔC_{ant} in the lower limb of AMOC. Therefore, the insufficient incorporation of the RCO
1030 in the GOBMs may also result in a lower CO_2 uptake, and at the same time also generates an excess
1031 CO_2 uptake in the NA SPSS (Aumont et al. 2001; Gao et al. 2023).

1032 4.5 Future recommendations

1033 Observations of pCO_2 in the Atlantic Ocean have greatly improved over the past two decades
1034 making it one of the most densely sampled oceans temporally and spatially. However, the surface
1035 pCO_2 observations are highly skewed in space and time, potentially inducing spurious results in the
1036 gap-filling algorithms used for estimating CO_2 fluxes. In fact, even in the well sampled Atlantic, the
1037 observations cover less than 10% of all $1^\circ \times 1^\circ$ by 1-month grid points, requiring the gap filling
1038 methods to fill more than 90% of the grid cells. Recent studies with synthetic model data using similar

1039 resolution and parameterizations to observations (Gloege et al., 2021; Hauck et al., 2023) indicate
1040 that gap-filling methods may be prone to a possible overestimation of the decadal rates of increase in
1041 CO₂ uptake when data are sparse, partially explaining the discrepancy between these products and
1042 GOBMs. We also note that in the data-sparse period 1985-2000, the trends generated by the various
1043 observation-based products were highly correlated with their flux estimate in 1985. This shows that
1044 with reduced observational coverage, the trend in the products tends to drift apart. Therefore, data-
1045 coverage as well as gap-filling methods need to be improved to reduce uncertainties in the trends. It
1046 is now quite worrisome that key Atlantic ship of opportunity lines for surface ocean pCO₂
1047 observations have been lost or operated with reduced capacity the past years - this tendency must be
1048 reversed if we want to retain our ability to accurately constrain the Atlantic Ocean CO₂ sink and its
1049 variability. Another aspect is the lack of funding in SOCAT itself, resulting in a longer time lag before
1050 collected data gets included in the database
1051 (https://www.ioccp.org/images/Gnews/2023_A_Case_for_SOCAT.pdf).

1052 This assessment relies on simple bulk flux formulations used in pCO₂-based products and
1053 GOBMs to determine FCO₂ from ΔfCO₂ fields with little regard to interfacial processes controlling
1054 gas fluxes. Gas transfer is based on a global parameterization with wind speed. Recent advances in
1055 direct flux estimates provide the opportunity to use regionally resolved gas transfer estimates
1056 (Blomquist et al., 2017; Butterworth et al. 2016). Yang et al. (2022) show clear regional variation in
1057 the K660-wind speed relationship, which can explain some of the regional differences observed
1058 between GOBMs and pCO₂ products. Near-surface CO₂ concentration gradients impact fluxes as well
1059 as shown herein by applying a cool skin effect. Further improvements in characterization of these
1060 gradients will improve the quantification of CO₂ fluxes (Dong et al. 2022). Of note is that the effect
1061 of gas transfer and near-surface gradients will be less in GOBMs than pCO₂ products because of the
1062 inherent feedback between fluxes and concentration gradients in GOBMs (Bellenger et al., 2023).

1063 The Atlantic Ocean is characterized by high temporal dynamics not only in the surface layer
1064 but also in the deep layers connecting the North Atlantic to the Southern Ocean through the deep
1065 western boundary current. This involves strong mesoscale and sub-mesoscale dynamic currents and
1066 structures. The effectiveness of GOBMs in representing dynamic climate change processes is highly
1067 dependent on their spatial and temporal resolutions. Current spatial resolution can barely reproduce
1068 the dynamics of strong CO₂ transports in the Atlantic, as well as ocean-coastal interactions.

1069 A number of future model improvements could further address or minimize the discrepancies
1070 in the interior C_{ant} inventory estimates. As simulations of the ocean biogeochemistry are strongly
1071 constrained by the performance of the physical model (Doney et al., 2004), more detailed assessments
1072 should be carried out of key physical dynamics that govern the surface to deep carbon transport, such
1073 as the representation of mode water, intermediate and deep waters in the North Atlantic (Racape et
1074 al., 2018). Assessment of GOBMs' ability to simulate observed episodic ventilation events and their
1075 impact on interior C_{ant}, e.g., as documented in Rhein et al. (2017) and Fröb et al. (2016), could shed
1076 additional light on their validity. Through winter convective mixing, biases in the interior carbon
1077 chemistry can influence the upper ocean carbon uptake capacity in models due to biases in the

1078 buffering capacity of the ocean (Vaithinada Ayar et al., 2022; Terhaar et al., 2022). Improvements in
1079 the representation of mixing by the models would likely also alleviate the issues with the simulated
1080 amplitude and timing of spring bloom and winter remineralization in the subpolar region (that we
1081 identified as key deficiencies in GOBMs) and further improve their FCO₂ seasonal cycle. Better
1082 observational constraints and improvement in mixing parameterizations are needed to alleviate this
1083 issue. Higher spatial resolution is likely necessary to improve key upper ocean physical features in
1084 the Atlantic Ocean such as the Gulf Stream (Chassignet et al., 2020), which has been shown to play
1085 a significant role in constraining the seasonality and trends of North Atlantic carbon fluxes and
1086 interior sequestration (Goris et al., 2023). Results from the high-resolution regional model (ROMS-
1087 ETHZ) indicate a better representation of the FCO₂ seasonal cycle in the NA SPSS and a better
1088 representation of the trends for 2001-2018 in NA SPSS, NA STSS and SA STPS, while we see no
1089 improvement or even a worse representation in other regions. A detailed and overarching
1090 investigation of the benefits of higher resolution for the carbon cycle would be desirable. Further, as
1091 the number of observations continue to increase, improvements in biogeochemical parameterizations
1092 can be achieved through data assimilation, e.g. to address the regionally heterogeneous biological
1093 processes (Tjiputra et al., 2007; Gharamti et al., 2017). In addition, improvement in biological model
1094 complexity may be needed to optimally reproduce the observed biogeochemical dynamics across
1095 spatially varying regimes such as the Atlantic basin (Gehlen et al., 2015). The interior lateral transport
1096 of C_{ant} is projected to play an increasing role in the future (Tjiputra et al., 2010). Better constraints of
1097 the northward (and southward) transport of anthropogenic CO₂ in the ocean, through the upper (and
1098 lower) limb of the AMOC should be considered to improve estimates of fluxes further north (Cainzos
1099 et al., 2022). Finally, an improved model experiment protocol that includes a multi-centennial
1100 preindustrial spin up (Seferian et al., 2016), common initialization procedure, and implementation of
1101 the river carbon loop should be considered (see also Terhaar et al., 2024).

1102 In the North Atlantic, Fontela et al., (2020) showed that semi-refractory DOC mineralization
1103 in the lower limb of AMOC represents a significant contribution to DIC of the same order of
1104 magnitude as CO₂ exchange with the atmosphere, resulting in a possible CO₂ source that could
1105 explain the differences observed between the observed FCO₂ (Takahashi et al., 2009) and those
1106 estimated by inverse methods (Mikaloff Fletcher et al., 2007; Gruber et al., 2009; Gerber et al., 2009).
1107 In RECCAP, the role of DOC has not been evaluated, nor the double impact of its seasonal cycle, i.e.
1108 diverting DIC which reduces pCO₂ in summer or by DOC deep mineralization, increasing DIC
1109 transport. The semi-refractory DOC is exported to the mesopelagic zone and even deeper depths in
1110 the North Atlantic, as documented by Hansell (2013), who estimated ~0.34 PgC yr⁻¹ DOC export,
1111 with a mineralization time scale to CO₂ of decades. In the North Atlantic the coupling between DOC
1112 production and export is revealed in the export of locally produced DOC (Roshan and DeVries, 2017;
1113 Fernandez-Castro et al., 2019). In fact, the carbon sequestration mediated by DOC has been shown
1114 to represent around a third of the North Atlantic CO₂ sink (Fontela et al., 2016). It has been
1115 demonstrated in DOC enrichment along the AMOC and its coupling with intense overturning in the
1116 NA SPSS leads to downward transport of 0.07 PgC yr⁻¹ associated mainly with water masses
1117 transported by the DWBC (Fontela et al., 2020). In addition, 0.09 PgC yr⁻¹ of DOC exported

1118 northward from the subtropics is mineralized in the deep layers of the AMOC. Inverse models do not
1119 include the DOC divergence which is assumed to be small (Mikaloff Fletcher et al., 2007). This
1120 carbon cycle component has not been evaluated neither in RECCAP1 nor in RECCAP2 and,
1121 considering the importance of its magnitude relative to FCO_2 , it is relevant to consider it in future
1122 biogeochemical modeling experiments together with other modeling improvements proposed here.
1123 Articles highlighting the importance of DOC in the carbon balance are relatively recent (Fontela et
1124 al. 2016; 2020), with global non-seasonal climatology (Roshan et DeVries, 2017) and the compilation
1125 of a global DOC database (Hansell et al. 2021) being very recent, making it difficult to assess DOC
1126 modeling in GOBMs.

1127

1128 **5 Conclusions**

1129 We provide here the current "best estimate" of surface CO_2 fluxes as well as the accumulation
1130 and transport of C_{ant} in the Atlantic, including the Mediterranean Sea for the RECCAP2 period, 1985-
1131 2018. For this estimate, we have compared different types of ocean biogeochemical models (GOBMs,
1132 ROBM, data-assimilated models) with various observation-based products. Our analysis includes
1133 several time-scales of variability.

1134 We find that the **mean** net sea-air CO_2 flux of the GOBM ensemble is 27% stronger than
1135 estimates from observation-based pCO_2 products. This difference is within the uncertainties of the
1136 GOBMs and pCO_2 products and can be explained, in part, by known discrepancies between pCO_2
1137 products and GOBMs. Specifically, this includes the oceanic CO_2 outgassing due to the impact of
1138 riverine discharge that is not explicitly represented in most GOBMs. The pCO_2 products may also be
1139 biased by not including near surface pCO_2 gradients. Adjusting for these effects mostly leads to higher
1140 fluxes into the ocean which — if applied to all pCO_2 products — would lead to better agreement
1141 between GOBMs and pCO_2 products for the time period considered here.

1142 The **trends** of sea-air CO_2 fluxes before and after year 2000 are similar across our ensemble
1143 of GOBMs (from -0.045 ± 0.012 to -0.060 ± 0.017 $PgC\text{-}yr^{-1} dec^{-1}$) and are consistent with the 43%
1144 increase in the atmospheric CO_2 growth rate between the pre-2000 period and the post-2000 period.
1145 In contrast, the trends obtained from surface CO_2 observations show a sharp increase from the trend
1146 of the pre-2000 of -0.024 ± 0.075 $PgC\text{-}yr^{-1} dec^{-1}$ to a trend of -0.126 ± 0.031 $PgC\text{-}yr^{-1} dec^{-1}$ in the post-
1147 2000 period.

1148 All biomes apart from the subpolar North Atlantic show a high correlation between GOBMs
1149 and pCO_2 products in terms of FCO_2 seasonality. In the North Atlantic subpolar biome, the GOBMs
1150 simulate a seasonal cycle driven predominantly by temperature variation, which the pCO_2 products
1151 do not show.

1152 Averaged over the Atlantic, the ensemble of GOBMs shows lower interannual variability
1153 (IAV) in FCO_2 than the pCO_2 products. Spatially, and temporally, pCO_2 products and GOBMs agree
1154 well in most of the Atlantic biomes but disagree quite substantially in the subpolar North Atlantic.

1155 Here, the variability of the GOBMs is mostly driven by SST variations, which is not the case for the
1156 pCO₂ products.

1157 The mean C_{ant} storage change between 1994-2007 simulated by the GOBM ensemble was
1158 found to be 28% lower than that estimated from DIC observations in the ocean interior and 25% lower
1159 than the data-assimilated model. These differences are higher than the standard deviation of the
1160 GOBMs estimates (17%). In contrast to the results described for the surface CO₂ fluxes, there is high
1161 agreement in anthropogenic CO₂ storage rates between GOBMs and those based on DIC observations
1162 in the NA SPSS and NA STSS biomes, whereas there are significant differences in the NA STPS,
1163 AEQU and SA STPS biomes, where the GOBM-estimates are on average 36% lower than
1164 observation-based estimates. The GOBMs indicate that 32% of the C_{ant} accumulating in the Atlantic
1165 comes from the Southern Ocean, in line with previous estimates from the literature. The
1166 Mediterranean Sea revealed an almost balanced net sea-air flux of CO₂, however it presented a C_{ant}
1167 accumulation of 0.018 PgC yr⁻¹, of which 70% are taken up from the atmosphere and 30% are
1168 imported from the Atlantic.

1169 Estimates of the land-to-ocean transport of carbon and nutrients indicate a significant and
1170 large net CO₂ outgassing due to the input of this terrestrially derived matter. The protocol of
1171 RECCAP2 recommended the use of the updated estimate of 0.65 PgC yr⁻¹ of Regnier et al. (2022) at
1172 the global level. For the Atlantic Ocean, the outgassing rates per square meter are twice the global
1173 rates when considering the spatial distribution of the riverine carbon outgassing (RCO) simulated by
1174 Lacroix et al. (2020). This RCO is especially significant in the NA STPS biome and hampers the
1175 comparison of GOBM and observation-based estimates of CO₂ fluxes, transport and accumulation.
1176 Therefore, it is essential to have more realistic models to better understand the influences of land-sea
1177 fluxes in the Atlantic Ocean and to be able to use observational-estimates with confidence when
1178 determining the accumulation of C_{ant}. This also requires better spatial and seasonal coverage of
1179 biogeochemical observations such as CO₂, nutrients and DOC to allow for improved model
1180 evaluation or even generate new emergent constraints.

1181

1182 **Acknowledgments**

1183 The authors have no conflicts of interest. We are grateful for the formal reviewer comments
1184 and suggestions provided by Yuanxu Dong and the associated editors. F. F Pérez and A. Velo were
1185 supported by the BOCATS2 (PID2019-104279GB-C21) project funded by
1186 MCIN/AEI/10.13039/501100011033, and with E. Huertas contributed to WATER:iOS CSIC PTI. M.
1187 Becker acknowledges funding from the Research Council of Norway through N-ICOS-2 (grant no
1188 296012), and Nansen Legacy, grant no. 276730. NGo was supported by the strategic project
1189 DYNASOR (DYnamics of the North Atlantic Surface and Overturning ciRculation) of the Bjerknes
1190 Centre for Climate Research. M. Lopez-Mozos was supported by the grant PRE2020-093138 funded

1191 by MCIN/AEI/ 10.13039/501100011033 and by “ESF Investing in your future”. J. Tjiputra
 1192 acknowledges funding from EU funded H2020 projects TRIATLAS (no. 817578) and OceanICU (no.
 1193 101083922). A. Olsen appreciates support from the Research Council of Norway through N-ICOS-2
 1194 (grant no 296012), and Horizon Europe through grant no. 101083922 (OceanICU Improving Carbon
 1195 Understanding). J.D. Muller, and N. Gruber acknowledge support from the European Union's
 1196 Horizon 2020 research and innovation program under grant agreement no. 821003 (project 4C) and
 1197 no. 820989 (project COMFORT). M. Gehlen acknowledges support from the European Union's
 1198 Horizon 2020 research and innovation program under grant agreements no. 820989 (project
 1199 COMFORT) and no. 862923 (project AtlantECO), as well as from Horizon Europe through grant no.
 1200 101083922 (OceanICU). T. Chau and M. Gehlen appreciate funding through the European
 1201 Copernicus Marine Environment Monitoring Service (CMEMS) grant no. 83-CMEMSTAC-MOB).
 1202 J. Hauck acknowledges funding from the Initiative and Networking Fund of the Helmholtz
 1203 Association (Helmholtz Young Investigator Group Marine Carbon and Ecosystem Feedbacks in the
 1204 Earth System [MarESys], grant number VH-NG-1301) and from ERC-2022-STG OceanPeak, grant
 1205 agreement 101077209

1206

1207 **Data Availability Statement**

1208 The RECCAP2 ocean data collection can be found in Müller (2023).

1209

1210 **References**

1211 Andrié, C., Oudot, C., Genthon, C., & Merlivat, L. (1986), CO₂ fluxes in the tropical Atlantic
 1212 during FOCAL cruises, *Journal of Geophysical Research*, 91(C10), 11741–11755,
 1213 <https://doi.org/10.1029/JC091iC10p11741>

1214 Álvarez, M., Ríos, A. F., Pérez, F. F., Bryden, H. L., & Rosón, G. (2003). Transports and budgets
 1215 of total inorganic carbon in the subpolar and temperate North Atlantic. *Global Biogeochemical*
 1216 *Cycles*, 17(1), 2-1. <https://doi.org/10.1029/2002GB001881>

1217 Aumont, O., Ethe, C., Tagliabue, A., Bopp, L., & Gehlen, M. (2015). PISCES-v2: an ocean
 1218 biogeochemical model for carbon and ecosystem studies. *Geoscientific Model Development*, 8,
 1219 2465-2513. <https://doi.org/10.5194/gmd-8-2465-2015>

1220 Aumont, O., Orr, J. C., Monfray, P., Ludwig, W., Amiotte-Suchet, P., & Probst, J.-L. (2001).
 1221 Riverine-driven interhemispheric transport of carbon, *Global Biogeochemical Cycles*, 15(2), 393–
 1222 405. <https://doi.org/10.1029/1999GB001238>

1223 Bakker, D. C. E., Pfeil, B., Landa, C. S., Metzl, N., O’Brien, K. M., Olsen, A., et al. (2016). A
 1224 multi-decade record of high-quality CO₂ data in version 3 of the Surface Ocean CO₂ Atlas
 1225 (SOCAT). *Earth System Science Data*, 8, 383–413. <https://doi.org/10.5194/essd-8-383-2016>

1226 Bakker, D. C. E., Alin, S. R., Becker, M., Bittig, H., Castaño-Primo, R., Feely, R. A., et al. (2022).
 1227 *SOCAT version 2022 for quantification of ocean CO₂ uptake*. Available at:

- 1228 https://www.socat.info/wp-content/uploads/2022/06/2022_Poster_SOCATv2022_release.pdf.
- 1229 Bates, N. R., Takahashi, T., Chipman, D. W., & Knap, A. H. (1998). Variability of pCO₂ on diel to
1230 seasonal timescales in the Sargasso Sea near Bermuda. *Journal of Geophysical Research: Oceans*,
1231 *103*(C8), 15567-15585. <https://doi.org/10.1029/98JC00247>
- 1232 Bates, N. R., Astor, Y. M., Church, M. J., Currie, K., Dore, J. E., González-Dávila, M., ... &
1233 Santana-Casiano, J. M. (2014). A time-series view of changing surface ocean chemistry due to
1234 ocean uptake of anthropogenic CO₂ and ocean acidification. *Oceanography*, *27*(1), 126-141.
1235 <http://www.jstor.org/stable/24862128>
- 1236 Becker, M., Steinhoff, T., & Körtzinger, A. (2018). A detailed view on the seasonality of stable
1237 carbon isotopes across the North Atlantic. *Global Biogeochemical Cycles*, *32*, 1406– 1419.
1238 <https://doi.org/10.1029/2018GB005905>
- 1239
- 1240 Bellenger, H., Bopp, L., Ethé, C., Ho, D., Duvel, J. P., Flavoni, S., et al. (2023). Sensitivity of the
1241 Global Ocean Carbon Sink to the Ocean Skin in a Climate Model. *Journal of Geophysical Research:*
1242 *Oceans*, *128*(7), 1-22. <https://doi.org/10.1029/2022JC019479>
- 1243 Blomquist, B. W., Brumer, S. E., Fairall, C. W., Huebert, B. J., Zappa, C. J., Brooks, I. M., et al.
1244 (2017). Wind Speed and Sea State Dependencies of Air-Sea Gas Transfer: Results From the High
1245 Wind Speed Gas Exchange Study (HiWinGS). *Journal of Geophysical Research: Oceans*, *122*(10),
1246 8034-8062. <https://doi.org/10.1002/2017JC013181>
- 1247 Bower, A., Lozier, S., Biastoch, A., Drouin, K., Foukal, N., Furey, H., ... & Zou, S. (2019).
1248 Lagrangian views of the pathways of the Atlantic Meridional Overturning Circulation. *Journal of*
1249 *Geophysical Research: Oceans*, *124*(8), 5313-5335. <https://doi.org/10.1029/2019JC015014>
- 1250 Brady, R. X., Lovenduski, N. S., Alexander, M. A., Jacox, M., & Gruber, N. (2019). On the role of
1251 climate modes in modulating the air–sea CO₂ fluxes in eastern boundary upwelling systems.
1252 *Biogeosciences*, *16*, 329–346. <https://doi.org/10.5194/bg-16-329-2019>
- 1253 Breeden, M. L., & McKinley, G. A. (2016). Climate impacts on multidecadal pCO₂ variability in
1254 the North Atlantic: 1948–2009. *Biogeosciences*, *13*(11), 3387-3396. <https://doi.org/10.5194/bg-13-3387-2016>
- 1255
- 1256 Brown, P. J., McDonagh, E. L., Sanders, R., Watson, A. J., Wanninkhof, R., King, B. A., et al.
1257 (2021). Circulation-driven variability of Atlantic anthropogenic carbon transports and uptake.
1258 *Nature Geosciences*, *14*, 571–577. <https://doi.org/10.1038/s41561-021-00774-5>
- 1259 Butterworth, B. J., & Miller, S. D. (2016). Air-sea exchange of carbon dioxide in the Southern
1260 Ocean and Antarctic marginal ice zone. *Geophys. Res. Lett.*, *43*.
1261 <https://doi.org/10.1002/2016GL069581>
- 1262 Caínzos, V., Velo, A., Pérez, F. F., & Hernández-Guerra, A. (2022). Anthropogenic carbon
1263 transport variability in the Atlantic Ocean over three decades. *Global Biogeochemical Cycles*, *36*,
1264 e2022GB007475. <https://doi.org/10.1029/2022GB007475>
- 1265 Chassignet, E. P., Yeager, S. G., Fox-Kemper, B., Bozec, A., Castruccio, F., Danabasoglu, G., et al.
1266 (2020). Impact of horizontal resolution on global ocean–sea ice model simulations based on the
1267 experimental protocols of the Ocean Model Intercomparison Project phase 2 (OMIP-2).
1268 *Geoscientific Model Development*, *13*, 4595–4637. <https://doi.org/10.5194/gmd-13-4595-2020>

- 1269 Chau, T. T. T., Gehlen, M., & Chevallier, F. (2022). A seamless ensemble-based reconstruction of
 1270 surface ocean pCO₂ and air–sea CO₂ fluxes over the global coastal and open oceans.
 1271 *Biogeosciences*, 19 (4), 1087–1109. <https://doi.org/10.5194/bg-19-1087-2022>
- 1272 Clement, D., & Gruber, N. (2018). The eMLR (C*) method to determine decadal changes in the
 1273 global ocean storage of anthropogenic CO₂. *Global Biogeochemical Cycles*, 32(4), 654–
 1274 679. <https://doi.org/10.1002/2017GB005819>
- 1275 Coppola, L., Diamond Riquier, E., & Carval, T. (2018). Dyfamed Observatory Data. SEANOE.
 1276 <https://doi.org/10.17882/43749>.
- 1277 Crisp, D., Dolman, H., Tanhua, T., McKinley, G. A., Hauck, J., Bastos, A., ... & Aich, V. (2022).
 1278 How well do we understand the land-ocean-atmosphere carbon cycle?. *Reviews of Geophysics*,
 1279 60(2), e2021RG000736. <https://doi.org/10.1029/2021RG000736>
- 1280 Denvil-Sommer, A., Gehlen, M., Vrac, M., & Mejia, C. (2019). LSCE-FFNN-v1: a two-step neural
 1281 network model for the reconstruction of surface ocean pCO₂ over the global
 1282 ocean. *Geoscientific Model Development*, 12(5), 2091-2105. [https://doi.org/10.5194/gmd-12-2091-](https://doi.org/10.5194/gmd-12-2091-2019)
 1283 [2019](https://doi.org/10.5194/gmd-12-2091-2019)
- 1284 De Carlo, E. H., Mousseau, L., Passafiume, O., Drupp, P. S., and Gattuso, J.-P. (2013). Carbonate
 1285 chemistry and air–sea CO₂ flux in a NW Mediterranean Bay over a four-year period: 2007–2011.
 1286 *Aquat. Geochem.* 19: 399–442. <https://doi.org/10.1007/s10498-013-9217-4>
- 1287 DeVries, T. (2014). The oceanic anthropogenic CO₂ sink: Storage, air-sea fluxes, and transports
 1288 over the industrial era. *Global Biogeochemical Cycles*, 28(7), 631-647.
 1289 <https://doi.org/10.1002/2013GB004739>
- 1290 DeVries, T. (2022). Atmospheric CO₂ and sea surface temperature variability cannot explain recent
 1291 decadal variability of the ocean CO₂ sink. *Geophysical Research Letters*, 49(7), e2021GL096018.
 1292 <https://doi.org/10.1029/2021GL096018>
- 1293 DeVries, T., Yamamoto, K., Wanninkhof, R., Gruber, N., Hauck, J., Müller, J. D. et al. (2023).
 1294 Magnitude, trends, and variability of the global ocean carbon sink from 1985-2018, *Global*
 1295 *Biogeochemical Cycles*, 37, e2023GB007780. <https://doi.org/10.1029/2023GB007780>
- 1296 Doney, S. C., Lindsay, K., Caldeira, K., Campin, J.-M., Drange, H., Dutay, J.-C., et al. (2004).
 1297 Evaluating global ocean carbon models: The importance of realistic physics. *Global*
 1298 *Biogeochemical Cycles*, 18, GB3017. <https://doi.org/10.1029/2003GB002150>
- 1299 Dong, Y., Bakker, D. C. E., Bell, T.G., Huang, B., Landschützer, P., Liss, P. S., & Yang, M. (2022).
 1300 Update on the temperature corrections of global air-sea CO₂ flux estimates. *Global Biogeochemical*
 1301 *Cycles*, 36, e2022GB007360. <https://doi.org/10.1029/2022GB007360>
- 1302 Fajar, N. M., Guallart, E. F., Steinfeldt, R., Ríos, A. F., Pelegrí, J. L., Pelejero, C., ... & Pérez, F. F.
 1303 (2015). Anthropogenic CO₂ changes in the equatorial Atlantic Ocean. *Progress in Oceanography*,
 1304 134, 256-270. <https://doi.org/10.1016/j.pocean.2015.02.004>
- 1305 Fay, A. R., & McKinley, G. A. (2014). Global open-ocean biomes: Mean and temporal variability.
 1306 *Earth System Science Data*, 6(2), 273–284. <https://doi.org/10.5194/essd-6-273-2014>
- 1307 Fay, A. R., Gregor, L., Landschützer, P., McKinley, G. A., Gruber, N., Gehlen, M., ... & Zeng, J.
 1308 (2021). SeaFlux: harmonization of air–sea CO₂ fluxes from surface pCO₂ data products using a
 1309 standardized approach. *Earth System Science Data*, 13(10), 4693-4710.

- 1310 <https://doi.org/10.5194/essd-13-4693-2021>
- 1311 Fernández-Castro, B., Álvarez, M., Nieto-Cid, M., Zunino, P., Mercier, H., & Álvarez-Salgado, X.
1312 A. (2019). Dissolved organic nitrogen production and export by meridional overturning in the
1313 eastern subpolar North Atlantic. *Geophysical Research Letters*, 46(7), 3832-3842.
1314 <https://doi.org/10.1029/2018GL080284>
- 1315 Fontela, M., García-Ibáñez, M. I., Hansell, D. A., Mercier, H., & Pérez, F. F. (2016). Dissolved
1316 organic carbon in the North Atlantic meridional overturning circulation. *Scientific reports*, 6(1),
1317 26931. <https://doi.org/10.1038/srep26931>
- 1318 Fontela, M., Pérez, F. F., Mercier, H., & Lherminier, P. (2020). North Atlantic Western Boundary
1319 Currents Are Intense Dissolved Organic Carbon Streams. *Frontiers in Marine Science*, 7, 593757.
1320 <https://doi.org/10.3389/fmars.2020.593757>
- 1321 Friedlingstein, P., Jones, M. W., O'Sullivan, M., Andrew, R. M., Bakker, D. C. E., Hauck, J., et al.
1322 (2022). Global Carbon Budget 2021. *Earth System Science Data*, 14, 1917–2005.
1323 <https://doi.org/10.5194/essd-14-1917-2022>
- 1324 Fröb, F., Olsen, A., Våge, K., Moore, K., Yashayaev, I., Jeansson, E., & Rajasakaren, B. (2016).
1325 Irminger Sea deep convection injects oxygen and anthropogenic carbon to the ocean interior. *Nature*
1326 *Communications*, 7, 13244. <https://doi.org/10.1038/ncomms13244>
- 1327 Fröb, F., Olsen, A., Becker, M., Chafik, L., Johannessen, T., Reverdin, G., & Omar, A. (2019).
1328 Wintertime fCO₂ Variability in the Subpolar North Atlantic Since 2004. *Geophysical Research*
1329 *Letter*, 46(3), 1580-1590. <https://doi.org/10.1029/2018gl080554>
- 1330 Gao, S., Schwinger, J., Tjiputra, J., Bethke, I., Hartmann, J., Mayorga, E., & Heinze, C. (2023).
1331 Riverine impact on future projections of marine primary production and carbon uptake.
1332 *Biogeosciences*, 20(1), 93-119. <https://doi.org/10.5194/bg-20-93-2023>
- 1333 Gerber, M., Joos, F., Vázquez-Rodríguez, M., Touratier, F., & Goyet, C. (2009). Regional air-sea
1334 fluxes of anthropogenic carbon inferred with an Ensemble Kalman Filter. *Global biogeochemical*
1335 *cycles*, 23(1). <https://doi.org/10.1029/2008GB003247>
- 1336 Gharamti, M., Tjiputra, J., Bethke, I., Samuelsen, A., Skjelvan, I., Bentsen, M., & Bertino, L.
1337 (2017). Ensemble data assimilation for ocean biogeochemical state and parameter estimation at
1338 different sites. *Ocean Modelling*, 112, 65-89. <https://doi.org/10.1016/j.ocemod.2017.02.006>
- 1339 Gehlen, M., Barciela, R., Bertino, L., Brasseur, P., Butenschön, M., Chai, F., et al. (2015). Building
1340 the capacity for forecasting marine biogeochemistry and ecosystems: recent advances and future
1341 developments, *Journal of Operational Oceanography*, 8, s168-s187.
1342 <https://doi.org/10.1080/1755876X.2015.1022350>
- 1343 Gloege, L., McKinley, G. A., Landschützer, P., Fay, A. R., Frölicher, T. L., Fyfe, J. C., et al.
1344 (2021). Quantifying errors in observationally based estimates of ocean carbon sink variability.
1345 *Global Biogeochemical Cycles*, 35(4), e2020GB006788. <https://doi.org/10.1029/2020GB006788>
- 1346 Goddijn-Murphy, L. M., Woolf, D. K., Land, P. E., Shutler, J. D., & Donlon, C. (2015). The
1347 OceanFlux Greenhouse Gases methodology for deriving a sea surface climatology of CO₂ fugacity
1348 in support of air–sea gas flux studies. *Ocean Science*, 11(4), 519-541. <https://doi.org/10.5194/os-11-519-2015>
- 1350 González-Dávila, M., Santana-Casiano, J. M., Rueda, M. J., & Llinás, O. (2010). The water column

- 1351 distribution of carbonate system variables at the ESTOC site from 1995 to 2004. *Biogeosciences*,
1352 7(10), 3067-3081. <https://doi.org/10.5194/bg-7-3067-2010>
- 1353 Gonzalez-Dávila, M., Santana Casiano, J. M., & Ucha, I. R. (2009). Seasonal variability of fCO₂ in
1354 the Angola-Benguela region. *Progress in Oceanography*, 83, 124–133.
1355 <https://doi.org/10.1016/j.pocean.2009.07.033>
- 1356 Goris, N., J. Tjiputra, J. Schwinger, and C. Heinze (2015). Responses of carbon uptake and oceanic
1357 pCO₂ to climate change in the North Atlantic: A model study with the Bergen Earth System Model.
1358 *Global Biogeochem. Cycles*, 29, 1567–1583, [doi:10.1002/2015GB005109](https://doi.org/10.1002/2015GB005109).
- 1359 Goris, N., Tjiputra, J. F., Olsen, A., Schwinger, J., Lauvset, S. K., and Jeansson, E. (2018)
1360 Constraining Projection-Based Estimates of the Future North Atlantic Carbon Uptake, *J. Climate*,
1361 31, 3959–3978, <https://doi.org/10.1175/JCLI-D-17-0564.1>
- 1362 Goris, N., Johannsen, K., and Tjiputra, J. (2023). The emergence of the Gulf Stream and interior
1363 western boundary as key regions to constrain the future North Atlantic carbon uptake. *Geosci.*
1364 *Model Dev.*, 16, 2095–2117, <https://doi.org/10.5194/gmd-16-2095-2023>
- 1365 Gregor, L., Lebehot, A. D., Kok, S., & Scheel Monteiro, P. M. (2019). A comparative assessment
1366 of the uncertainties of global surface ocean CO₂ estimates using a machine-learning ensemble
1367 (CSIR-ML6 version 2019a)–have we hit the wall?. *Geoscientific Model Development*, 12(12),
1368 5113-5136. <https://doi.org/10.5194/gmd-12-5113-2019>
- 1369 Gregor, L., & Gruber, N. (2021). OceanSODA-ETHZ: a global gridded data set of the surface
1370 ocean carbonate system for seasonal to decadal studies of ocean acidification. *Earth System Science*
1371 *Data*, 13(2), 777-808. <https://doi.org/10.5194/essd-13-777-2021>
- 1372 Gruber, N., Keeling, C. D., & Stocker, T. F. (1998). Carbon-13 constraints on the seasonal
1373 inorganic carbon budget at the BATS site in the northwestern Sargasso Sea. *Deep Sea Research*
1374 *Part I: Oceanographic Research Papers*, 45(4-5), 673-717. [https://doi.org/10.1016/S0967-](https://doi.org/10.1016/S0967-0637(97)00098-8)
1375 [0637\(97\)00098-8](https://doi.org/10.1016/S0967-0637(97)00098-8)
- 1376 Gruber, N., Keeling, C. D., & Bates, N. R. (2002). Interannual variability in the North Atlantic
1377 Ocean carbon sink. *Science*, 298(5602), 2374-2378. <https://doi.org/10.1126/science.1077077>
- 1378 Gruber, N., Clement, D., Carter, B. R., Feely, R. A., van Heuven, S., Hoppema, M., et al. (2019).
1379 The oceanic sink for anthropogenic CO₂ from 1994 to 2007. *Science*, 363(6432), 1193–1199.
1380 <https://doi.org/10.1126/science.aau5153>
- 1381 Gruber, N., Gloor, M., Mikaloff Fletcher, S. E., Doney, S. C., Dutkiewicz, S., Follows, M. J., ... &
1382 Takahashi, T. (2009). Oceanic sources, sinks, and transport of atmospheric CO₂. *Global*
1383 *biogeochemical cycles*, 23(1) GB1005. <https://doi.org/10.1029/2008GB003349>
- 1384 Haine, T. W. N. (2016), Vagaries of Atlantic overturning, *Nat. Geosci.*, 9, 479– 480.
1385 <https://www.nature.com/articles/ngeo2748>
- 1386 Hansell, D. A. (2013). Recalcitrant dissolved organic carbon fractions. *Annual review of marine*
1387 *science*, 5, 421-445. [https://www.annualreviews.org/doi/abs/10.1146/annurev-marine-120710-](https://www.annualreviews.org/doi/abs/10.1146/annurev-marine-120710-100757)
1388 [100757](https://www.annualreviews.org/doi/abs/10.1146/annurev-marine-120710-100757)
- 1389 Hansell, D.A., Carlson, C.A., Amon, R.M. W., Álvarez-Salgado, X. A., Yamashita, Y., Romera-
1390 Castillo, C., Bif, M. B. (2021). Compilation of dissolved organic matter (DOM) data obtained from
1391 the global ocean surveys from 1994 to 2021 (NCEI Accession 0227166). NOAA National Centers

- 1392 for Environmental Information. Dataset. doi.org/10.25921/s4f4-ye35
- 1393 Hassoun, A. E. R., Gemayel, E., Krasakopoulou, E., Goyet, C., Saab, M. A.-A., Guglielmi, V., et al.
1394 (2015). Acidification of the Mediterranean Sea from anthropogenic carbon penetration. *Deep Sea*
1395 *Res. Pt. I Oceanogr Res Pap* 102:115. <http://doi.org/10.1016/j.dsr.2015.04.005>.
- 1396 Hauck, J. and Völker, C. (2015). Rising atmospheric CO₂ leads to large impact of biology on
1397 Southern Ocean CO₂ uptake via changes of the Revelle factor. *Geophys. Res. Lett.*, 42: 1459– 1464.
1398 doi: [10.1002/2015GL063070](https://doi.org/10.1002/2015GL063070).
- 1399 Hauck, J., Zeising, M., Le Quéré, C., Gruber, N., Bakker, D. C. E., Bopp, L., et al. (2020).
1400 Consistency and Challenges in the Ocean Carbon Sink Estimate for the Global Carbon Budget.
1401 *Frontiers in Marine Science*, 7(October), 1–22. <https://doi.org/10.3389/fmars.2020.571720>
- 1402 Hauck, J., Nissen, C., Landschützer, P., Rödenbeck, C., Bushinsky, S. & Olsen, A. (2023). Sparse
1403 observations induce large biases in estimates of the global ocean CO₂ sink: an ocean model
1404 subsampling experiment. *Phil. Trans. R. Soc. A.*, 381, 20220063.
1405 <http://doi.org/10.1098/rsta.2022.0063>
- 1406 Hauck, J., Gregor, L., Nissen, C., Patara, L., Hague, M., Mongwe, N. P., et al. (2023). The Southern
1407 Ocean carbon cycle 1985-2018: mean, seasonal cycle, trends and storage. *Global Biogeochemical*
1408 *Cycles*, 37, e2023GB007848. <https://doi.org/10.1029/2023GB007848>.
- 1409 Hirschi, J. J.-M., Barnier, B., Böning, C., Biastoch, A., Blaker, A. T., Coward, A., et al. (2020). The
1410 Atlantic meridional overturning circulation in high-resolution models. *Journal of Geophysical*
1411 *Research: Oceans*, 125, e2019JC015522. <https://doi.org/10.1029/2019JC015522>
- 1412 Ho, D. T., Law, C. S., Smith, M. J., Schlosser, P., Harvey, M., & Hill, P. (2006). Measurements of
1413 air-sea gas exchange at high wind speeds in the Southern Ocean: Implications for global
1414 parameterizations. *Geophysical Research Letters*, 33(16). <https://doi.org/10.1029/2006GL026817>
- 1415 Holfort, J., Johnson, K. M., Schneider, B., Siedler, G., & Wallace, D. W. (1998). Meridional
1416 transport of dissolved inorganic carbon in the South Atlantic Ocean. *Global Biogeochemical Cycles*,
1417 *12*(3), 479-499. <https://doi.org/10.1029/98GB01533>
- 1418 Huertas, I. E., Ríos, A. F., García-Lafuente, J., Makaoui, A., Rodríguez-Gálvez, S., Sánchez-
1419 Román, A., ... & Pérez, F. F. (2009). Anthropogenic and natural CO₂ exchange through the Strait
1420 of Gibraltar. *Biogeosciences*, 6(4), 647-662. <https://doi.org/10.5194/bg-6-647-2009>
- 1421 Iida, Y., Takatani, Y., Kojima, A., & Ishii, M. (2021). Global trends of ocean CO₂ sink and ocean
1422 acidification: an observation-based reconstruction of surface ocean inorganic carbon variables.
1423 *Journal of Oceanography*, 77, 323-358. <https://doi.org/10.1007/s10872-020-00571-5>
- 1424 Ibánhez, J. S. P., Araujo, M., & Lefèvre, N. (2016). The overlooked tropical oceanic CO₂ sink.
1425 *Geophysical Research Letter*, 43, 3804–3812. <https://doi.org/10.1002/2016GL068020>
- 1426 Ingrosso, G., Giani, M., Comici, C., Kralj, M., Piacentino, S., De Vittor, C., et al. (2016) Drivers of
1427 the carbonate system seasonal variations in a Mediterranean gulf. *Estuar. Coast. Shelf Sci.* 168: 58–
1428 70. <http://doi.org/10.1016/j.ecss.2015.11.001>
- 1429 Ito, R. G., Schneider, B., & Thomas, H. (2005). Distribution of surface fCO₂ and air-sea fluxes in
1430 the Southwestern subtropical Atlantic and adjacent continental shelf. *Journal of Marine Systems*.
1431 56, 227– 242. <https://doi.org/10.1016/j.jmarsys.2005.02.005>

- 1432 Jacobson, A. R., Mikaloff Fletcher, S. E., Gruber, N., Sarmiento, J. L., & Gloor, M. (2007). A joint
1433 atmosphere-ocean inversion for surface fluxes of carbon dioxide: 2. Regional results. *Global*
1434 *Biogeochemical Cycles*, 21(1) <https://doi.org/10.1029/2006GB002703>
- 1435 Jeansson, E., Olsen, A., Eldevik, T., Skjelvan, I., Omar, A. M., Lauvset, S. K., et al. (2011). The
1436 Nordic Seascarbon budget: Sources, sinks, and uncertainties. *Global Biogeochemical Cycles*, 25(4),
1437 GB4010. <https://doi.org/10.1029/2010GB003961>
- 1438 Jing, Y., Li, Y., Xu, Y. & Fan, G. (2019). Influences of the NAO on the North Atlantic CO₂ Fluxes
1439 in Winter and Summer on the Interannual Scale. *Adv. Atmos. Sci.* 36, 1288–1298.
1440 <https://doi.org/10.1007/s00376-019-8247-2>
- 1441 Kapsenberg, L., Alliouane, S., Gazeau, F., Mousseau, L., & Gattuso, J.-P. (2017). Coastal ocean
1442 acidification and increasing total alkalinity in the northwestern Mediterranean Sea. *Ocean Science*
1443 13, 411–426. <https://doi.org/10.5194/os-13-411-2017>
- 1444 Keeling, C. D. (1993). Lecture 2: Surface ocean CO₂. In *The global carbon cycle* (pp. 413-429).
1445 Springer Berlin Heidelberg. https://doi.org/10.1007/978-3-642-84608-3_17
- 1446 Keeling, R. F. & Peng, T-H. (1995). Transport of heat, CO₂ and O₂ by the Atlantic's thermohaline
1447 circulation. *Philosophical Transactions of the Royal Society of London B*, 348, 133-142.
1448 <https://doi.org/10.1098/rstb.1995.0055>
- 1449 Khatiwala, S., Primeau, F., & Hall, T. (2009). Reconstruction of the history of anthropogenic CO₂
1450 concentrations in the ocean. *Nature*, 462(7271), 346-349. <https://doi.org/10.1038/nature08526>
- 1451 Khatiwala, S., Tanhua, T., Mikaloff Fletcher, S., Gerber, M., Doney, S. C., Graven, H. D., ... &
1452 Sabine, C. L. (2013). Global ocean storage of anthropogenic carbon. *Biogeosciences*, 10(4), 2169-
1453 2191. <https://doi.org/10.5194/bg-10-2169-2013>
- 1454 Koseki, S., Tjiputra, J., Fransner, F., Crespo, L. R. & Keenlyside, N. S. (2023). Disentangling the
1455 impact of Atlantic Niño on sea-air CO₂ flux. *Nat Commun* 14, 3649.
1456 <https://doi.org/10.1038/s41467-023-38718-9>
- 1457 Körtzinger, A. (2003). A significant CO₂ sink in the tropical Atlantic Ocean associated with the
1458 Amazon River plume. *Geophysical Research Letter*, 30(24), 2287.
1459 <https://doi.org/10.1029/2003GL018841>
- 1460 Krasakopoulou E., Rapsomanikis, S., Papadopoulos, A., Papathanassiou, E. (2009) Partial pressure
1461 and air-sea CO₂ flux in the Aegean Sea during February 2006. *Cont Shelf Res*, 29: 1477-1488.
1462 <https://doi.org/10.1016/j.csr.2009.03.015>
- 1463 Krasakopoulou, E., Souvermezoglou, E., Goyet, C. (2017). Carbonate system parameters and
1464 anthropogenic CO₂ in the North Aegean Sea during October 2013. *Cont Shelf Res* 149: 69-81.
1465 <https://doi.org/10.1016/j.csr.2017.04.002>
- 1466 Lacroix, F., Ilyina, T., & Hartmann, J. (2020). Oceanic CO₂ outgassing and biological production
1467 hotspots induced by pre-industrial river loads of nutrients and carbon in a global modeling
1468 approach. *Biogeosciences*, 17(1), 55-88. <https://doi.org/10.5194/bg-17-55-2020>
- 1469 Landschützer, P., Gruber, N., E. Bakker, D. C., & Schuster, U. (2014), Recent variability of the
1470 global ocean carbon sink, *Global Biogeochemical Cycles*, 28, 927– 949.
1471 <https://doi.org/10.1002/2014GB004853>

- 1472 Lefèvre, N., Diverrès, D., & Gallois, F. (2010). Origin of CO₂ undersaturation in the western
1473 tropical Atlantic, *Tellus B*, 62(5), 595–607, <https://doi.org/10.1111/j.1600-0889.2010.00475.x>
- 1474 Leseurre, C., Lo Monaco, C., Reverdin, G., Metzl, N., Fin, J., Olafsdottir, S., & Racapé, V. (2020).
1475 Ocean carbonate system variability in the North Atlantic Subpolar surface water (1993–2017).
1476 *Biogeosciences*, 17(9), 2553–2577. <https://doi.org/10.5194/bg-17-2553-2020>
- 1477 Le Quéré, C., Andrew, R. M., Friedlingstein, P., Sitch, S., Hauck, J., Pongratz, J., et al. (2018),
1478 Global Carbon Budget. *Earth Syst. Sci. Data*, 10, 2141–2194. [https://doi.org/10.5194/essd-10-2141-](https://doi.org/10.5194/essd-10-2141-2018)
1479 [2018](https://doi.org/10.5194/essd-10-2141-2018)
- 1480 Louchard, D., Gruber, N., & Münnich, M. (2021). The Impact of the Amazon on the Biological
1481 Pump and the Air-Sea CO₂ Balance of the Western Tropical Atlantic. *Global Biogeochemical*
1482 *Cycles*, 35(6). <https://doi.org/10.1029/2020GB006818>
- 1483 Ma, X., Jing, Z., Chang, P., Liu, X., Montuoro, R., Small, R. J., ... & Wu, L. (2016). Western
1484 boundary currents regulated by interaction between ocean eddies and the atmosphere. *Nature*,
1485 535(7613), 533–537. <https://doi.org/10.1038/nature18640>
- 1486 Macdonald, A. M., Baringer, M. O., Wanninkhof, R., Lee, K. & Wallace, D. W. R. (2003). A
1487 1998_1992 comparison of inorganic carbon and its transport across 24.5°N in the Atlantic. *Deep-*
1488 *Sea Research. II*, 50, 3041–3064 (2003). <https://doi.org/10.1016/j.dsr2.2003.07.009>
- 1489 Macovei, V. A., Hartman, S. E., Schuster, U., Torres-Valdés, S., Moore, C. M., & Sanders, R. J.
1490 (2020). Impact of physical and biological processes on temporal variations of the ocean carbon sink
1491 in the mid-latitude North Atlantic (2002–2016). *Progress in Oceanography*, 180, 102223
1492 <https://doi.org/10.1016/j.pocean.2019.102223>
- 1493 McKinley, G. A., Fay, A. R., Eddebar, Y. A., Gloege, L., & Lovenduski, N. S. (2020). External
1494 forcing explains recent decadal variability of the ocean carbon sink. *AGU Advances*, 1(2),
1495 e2019AV000149. <https://doi.org/10.1029/2019AV000149>
- 1496 McKinley, G. A., Ritzer, A. L., & Lovenduski, N. S. (2018). Mechanisms of northern North
1497 Atlantic biomass variability. *Biogeosciences*, 15, 6049–6066, [https://doi.org/10.5194/bg-15-6049-](https://doi.org/10.5194/bg-15-6049-2018)
1498 [2018](https://doi.org/10.5194/bg-15-6049-2018)
- 1499 Michaels, A. F., Bates, N. R., Buesseler, K. O., Carlson, C. A., & Knap, A. H. (1994). Carbon-cycle
1500 imbalances in the Sargasso Sea. *Nature*, 372(6506), 537–540. <https://doi.org/10.1038/372537a0>
- 1501 Mikaloff Fletcher, S. E., Gruber, N., Jacobson, A. R., Doney, S. C., Dutkiewicz, S., Gerber, M., et
1502 al. (2006). Inverse estimates of anthropogenic CO₂ uptake, transport, and storage by the ocean.
1503 *Global Biogeochemical Cycles*, 20(2), GB2002. <https://doi.org/10.1029/2005GB002530>
- 1504 Mikaloff-Fletcher, S. E., Gruber, N., Jacobson, A. R., Gloor, M., Doney, S. C., Dutkiewicz, S., et
1505 al. (2007). Inverse estimates of the oceanic sources and sinks of natural CO₂ and the implied
1506 oceanic carbon transport. *Global Biogeochemical Cycles*, 21, GB1010 (2007).
1507 <https://doi.org/10.1029/2006GB002751>
- 1508 Müller, J. D. (2023). RECCAP2-ocean data collection [Dataset]. Zenodo.
1509 <https://doi.org/10.5281/zenodo.7990823>
- 1510 Muller, J. D., Gruber, N., Carter, B., Feely, R., Ishii, M., Lange, N., et al. (2023). Decadal trends in
1511 the oceanic storage of anthropogenic carbon from 1994 to 2014. *AGU Advances*, 4,
1512 e2023AV000875. <https://doi.org/10.1029/2023AV000875>

- 1513 Nightingale, P. D., Malin, G., Law, C. S., Watson, A. J., Liss, P. S., Liddicoat, M. I., Boutin, J. &
1514 Upstill-Goddard, R. C. (2000). In situ evaluation of air-sea gas exchange parameterizations using
1515 novel conservative and volatile tracers. *Global Biogeochemical Cycles*, 14(1), 373-387,
1516 <https://doi.org/10.1029/1999GB900091>
- 1517 Olsen, A., Key, R. M., Van Heuven, S., Lauvset, S. K., Velo, A., Lin, X., ... & Suzuki, T. (2016).
1518 The Global Ocean Data Analysis Project version 2 (GLODAPv2)—an internally consistent data
1519 product for the world ocean. *Earth System Science Data*, 8(2), 297-323.
1520 <https://doi.org/10.5194/essd-8-297-2016>
- 1521 Olsen, A., Brown, K. R., Chierici, M., Johannessen, T., & Neill, C. (2008). Sea-surface CO₂
1522 fugacity in the subpolar North Atlantic. *Biogeosciences*, 5(2), 535-547. [https://doi.org/10.5194/bg-](https://doi.org/10.5194/bg-5-535-2008)
1523 [5-535-2008](https://doi.org/10.5194/bg-5-535-2008)
- 1524 Olsen, A., Lange, N., Key, R. M., Tanhua, T., Álvarez, M., Becker, S., ... & Wanninkhof, R. (2019).
1525 GLODAPv2. 2019—an update of GLODAPv2. *Earth System Science Data*, 11(3), 1437-
1526 1461. <https://doi.org/10.5194/essd-11-1437-2019>
- 1527 Padin, X. A., Vazquez-Rodriguez, M., Castaño, M., Velo, A., Alonso-Perez, F., Gago, J., et al.
1528 (2010). Air-Sea CO₂ fluxes in the Atlantic as measured during boreal spring and autumn.
1529 *Biogeosciences*, 7, 1587–1606. <https://doi.org/10.5194/bg-7-1587-2010>
- 1530 Park, G. -H., Wanninkhof, R., Doney, S. C., Takahashi, T., Lee, K., Feely, R. A., et al. (2010).
1531 Variability of global net sea–air CO₂ fluxes over the last three decades using empirical
1532 relationships. *Tellus B*, 62, 352-368. <https://doi.org/10.1111/j.1600-0889.2010.00498.x>
- 1533 Petihakis, G., Perivoliotis, L., Korres, G., Ballas, D., Frangoulis, C., Pagonis, P., ... & Zisis, N.
1534 (2018). An integrated open-coastal biogeochemistry, ecosystem and biodiversity observatory of the
1535 eastern Mediterranean—the Cretan Sea component of the POSEIDON system. *Ocean Science*, 14(5),
1536 1223-1245. <https://doi.org/10.5194/os-14-1223-2018>
- 1537 Pérez, F. F., Vázquez-Rodríguez, M., Louarn, E., Padín, X. A., Mercier, H., & Ríos, A. F. (2008).
1538 Temporal variability of the anthropogenic CO₂ storage in the Irminger Sea. *Biogeosciences*, 5(6),
1539 1669-1679. <https://doi.org/10.5194/bg-5-1669-2008>
- 1540 Pérez, F. F., Mercier, H., Vázquez-Rodríguez, M., Lherminier, P., Velo, A., Pardo, P. C., et al.
1541 (2013). Atlantic Ocean CO₂ uptake reduced by weakening of the meridional overturning circulation.
1542 *Nature Geoscience*, 6(2), 146–152. <https://doi.org/10.1038/ngeo1680>
- 1543 Pfeil B., Olsen, A., Bakker, D. C. E., Hankin, S., Koyuk, H., Kozyr, A., et al. (2013). A uniform,
1544 quality controlled surface ocean CO₂ atlas (SOCAT). *Earth System Science Data*, 5, 125–143.
1545 <https://doi.org/10.5194/essd-5-125-2013>
- 1546 Racapé, V., Zunino, P., Mercier, H., Lherminier, P., Bopp, L., Pérez, F. F., & Gehlen, M. (2018).
1547 Transport and storage of anthropogenic C in the North Atlantic Subpolar Ocean. *Biogeosciences*,
1548 15(14), 4661–4682. <https://doi.org/10.5194/bg-15-4661-2018>
- 1549 Regnier, P., Resplandy, L., Najjar, R. G., & Ciais, P. (2022). The land-to-ocean loops of the global
1550 carbon cycle. *Nature*, 603(7901), 401-410. <https://doi.org/10.1038/s41586-021-04339-9>
- 1551 Regnier, P., Friedlingstein, P., Ciais, P., Mackenzie, F. T., Gruber, N., Janssens, I. a., et al. (2013).
1552 Anthropogenic perturbation of the carbon fluxes from land to ocean. *Nature Geoscience*, 6(8), 597–
1553 607. <https://doi.org/10.1038/ngeo1830>

- 1554 Resplandy, L., Keeling, R. F., Rödenbeck, C., Stephens, B. B., Khatiwala, S., Rodgers, K. B., et
 1555 al.(2018). Revision of global carbon fluxes based on a reassessment of oceanic and riverine carbon
 1556 transport. *Nature Geoscience*, 11 , 504–509. <https://doi.org/10.1038/s41561-018-0151-3>
- 1557 Rhein, M., D. Kieke, and R. Steinfeldt (2015), Advection of North Atlantic Deep Water from the
 1558 Labrador Sea to the southern hemisphere, *J. Geophys.Res. Oceans*, 120, 2471–2487,
 1559 <https://doi.org/10.1002/2014JC010605>
- 1560 Rhein, M., Steinfeldt, R., Kieke, D., Stendardo, I., & Yashayaev, I. (2017). Ventilation variability
 1561 of Labrador Sea Water and its impact on oxygen and anthropogenic carbon: a review. *Philosophical*
 1562 *Transactions A*, 375, 20160321. <http://dx.doi.org/10.1098/rsta.2016.0321>
- 1563 Ríos, A. F., Álvarez-Salgado, X. A., Pérez, F. F., Bingler, L. S., Arístegui, J., & Mémery, L. (2003).
 1564 Carbon dioxide along WOCE line A14: Water masses characterization and anthropogenic entry.
 1565 *Journal of Geophysical Research: Oceans*, 108(C4). <https://doi.org/10.1029/2000JC000366>
- 1566 Ríos, A. F., Velo, A., Pardo, P. C., Hoppema, M., & Pérez, F. F. (2012). An update of
 1567 anthropogenic CO₂ storage rates in the western South Atlantic basin and the role of Antarctic
 1568 Bottom Water. *Journal of Marine Systems*, 94, 197-
 1569 203. <https://doi.org/10.1016/j.jmarsys.2011.11.023>
- 1570 Rödenbeck et al., 2014, Rödenbeck, C., Bakker, D. C. E., Metzl, N., Olsen, A., Sabine, C., Cassar,
 1571 N., Reum, F., Keeling, R. F., and Heimann, M.(2014) Interannual sea–air CO₂ flux variability from
 1572 an observation driven ocean mixed-layer scheme, *Biogeosciences*, 11, 4599–4613,
 1573 <https://doi.org/10.5194/bg-11-4599-2014>
- 1574 Rödenbeck, C., Bakker, D. C. E., Gruber, N., Iida, Y., Jacobson, A. R., Jones, S., et al. (2015).
 1575 Data-based estimates of the ocean carbon sink variability – first results of the Surface Ocean pCO₂
 1576 Mapping intercomparison (SOCOM), *Biogeosciences*, 12, 7251– 7278, [https://doi.org/10.5194/bg-](https://doi.org/10.5194/bg-12-7251-2015)
 1577 [12-7251-2015](https://doi.org/10.5194/bg-12-7251-2015)
- 1578 Rödenbeck, C., DeVries, T., Hauck, J., Le Quéré, C., & Keeling, R. F. (2022). Data-based estimates
 1579 of interannual sea–air CO₂ flux variations 1957–2020 and their relation to environmental drivers.
 1580 *Biogeosciences*, 19, 2627–2652, <https://doi.org/10.5194/bg-19-2627-2022>
- 1581 Rödenbeck, C., Keeling, R. F., Bakker, D. C. E., Metzl, N., Olsen, A., Sabine, C., & Heimann, M.
 1582 (2013). Global surface-ocean pCO₂ and sea–air CO₂ flux variability from an observation-driven ocean
 1583 mixed-layer scheme, *Ocean Sciences*, 9, 193–216. <https://doi.org/10.5194/os-9-193-2013>
- 1584 Rodgers, K. B., Schwinger, J., Fassbender, A. J., Landschützer, P., Yamaguchi, R., Frenzel, H., et
 1585 al. (2023). Seasonal variability of the surface ocean carbon cycle: a synthesis. *Global*
 1586 *Biogeochemical Cycles*, 37, e2023GB007798. <https://doi.org/10.1029/2023GB007798>
- 1587 Roshan, S., & DeVries, T. (2017). Efficient dissolved organic carbon production and export in the
 1588 oligotrophic ocean. *Nature communications*, 8(1), 2036. [https://doi.org/10.1038/s41467-017-02227-](https://doi.org/10.1038/s41467-017-02227-3)
 1589 [3](https://doi.org/10.1038/s41467-017-02227-3)
- 1590 Rosón, G. (2003). Carbon distribution, fluxes, and budgets in the subtropical North Atlantic Ocean
 1591 (24.5°N). *Journal of Geophysical Research*, 108(C5), 3144. <https://doi.org/10.1029/1999JC000047>
- 1592 Sabine, C. L., Hankin, S., Koyuk, H., Bakker, D. C. E., Pfeil, B., Olsen, A., et al. (2013). Surface
 1593 ocean CO₂ Atlas (SOCAT) gridded data products. *Earth System Science.Data*, 5, 145–153.
 1594 <https://doi.org/10.5194/essd-5-145-2013>

- 1595 Sabine, C. L., Feely, R. A., Gruber, N., Key, R. M., Lee, K., Bullister, J. L., et al. (2004). The
 1596 Oceanic Sink for Anthropogenic CO₂, *Science*, 305, 367–371, 2004.
 1597 <https://doi.org/10.1126/science.1097403>
- 1598 Santana-Casiano, J. M., González-Dávila, M., Rueda, M., Llinás, O., and González-Dávila, E.-
 1599 F.(2007).: The interannual variability of oceanic CO₂ parameters in the northeast Atlantic
 1600 subtropical gyre at the ESTOC site, *Global Biogeochem. Cy.*, 21, GB1015,
 1601 <https://doi.org/10.1029/2006GB002788>
- 1602 Santana-Casiano, J. M., González-Dávila, M., & Ucha, I. R. (2009). Carbon dioxide fluxes in the
 1603 Benguela upwelling system during winter and spring: A comparison between 2005 and 2006. *Deep*
 1604 *Sea Research Part II: Topical Studies in Oceanography*, 56(8-10), 533-541.
 1605 <https://doi.org/10.1016/j.dsr2.2008.12.010>
- 1606 Schneider, A., Tanhua, T., Körtzinger, A., & Wallace, D. W. (2010). High anthropogenic carbon
 1607 content in the eastern Mediterranean. *Journal of Geophysical Research: Oceans*, 115(C12).
 1608 <https://doi.org/10.1029/2010JC006171>
- 1609 Schuster, U., McKinley, G. A., Bates, N., Chevallier, F., Doney, S. C., Fay, A. R., et al. (2013). An
 1610 assessment of the Atlantic and Arctic sea–air CO₂ fluxes, 1990–2009. *Biogeosciences*, 10, 607–
 1611 627, <https://doi.org/10.5194/bg-10-607-2013>
- 1612 Schwinger, J., Goris, N., Tjiputra, J. F., Kriest, I., Bentsen, M., Bethke, I., et al. (2016). Evaluation
 1613 of NorESM-OC (versions 1 and 1.2), the ocean carbon-cycle stand-alone configuration of the
 1614 Norwegian Earth System Model (NorESM1). *Geoscientific Model Development*, 9(8), 2589-2622.
 1615 <https://doi.org/10.5194/gmd-9-2589-2016>
- 1616 Séférian, R., Gehlen, M., Bopp, L., Resplandy, L., Orr, J. C., Marti, O., et al. (2016). Inconsistent
 1617 strategies to spin up models in CMIP5: implications for ocean biogeochemical model performance
 1618 assessment, *Geoscientific Model Development*, 9, 1827–1851. [https://doi.org/10.5194/gmd-9-1827-](https://doi.org/10.5194/gmd-9-1827-2016)
 1619 [2016](https://doi.org/10.5194/gmd-9-1827-2016)
- 1620 Séférian, R., Berthet, S., Yool, A., Palmieri, J., Bopp, L., Tagliabue, A., et al. (2020). Tracking
 1621 Improvement in Simulated Marine Biogeochemistry Between CMIP5 and CMIP6. *Current Climate*
 1622 *Change Reports*, 6, 95–119. <https://doi.org/10.1007/s40641-020-00160-0>
- 1623 Sisma-Ventura, G., Or, B. M., Yam, R., Herut, B., & Silverman, J. (2017) pCO₂ variability in the
 1624 surface waters of the ultra-oligotrophic Levantine Sea: exploring the air-sea CO₂ fluxes in a fast
 1625 warming region. *Mar. Chem.* 196: 13–23. <https://doi.org/10.1016/j.marchem.2017.06.006>
- 1626 Steinfeldt, R., Rhein, M., Bullister, J. L., & Tanhua, T. (2009) Inventory changes in anthropogenic
 1627 carbon from 1997–2003 in the Atlantic Ocean between 20°S and 65°N. *Global Biogeochemical*
 1628 *Cycles*, 23, GB3010. <https://doi.org/10.1029/2008GB003311>
[2008GB003311](https://doi.org/10.1029/2008GB003311)
- 1629 Stöven T. and T. Tanhua, (2014) Ventilation of the Mediterranean Sea constrained by multiple
 1630 transient tracer measurements. *Ocean Sci.*, 10, 439–457, <https://doi.org/10.5194/os-10-439-2014>
- 1631 Sarmiento, J. L., & Sundquist, E. T. (1992). Revised budget for the oceanic uptake of anthropogenic
 1632 carbon dioxide. *Nature*, 356(6370), 589-593. <https://doi.org/10.1038/356589a0>
- 1633 Takahashi, T. (1961). Carbon dioxide in the atmosphere and Atlantic Ocean water. *Journal of*
 1634 *Geophysical. Research.*, 66, 477-494. <https://doi.org/10.1029/JZ066i002p00477>
- 1635 Takahashi, T., Olafsson, J., Goddard, J., Chipman, D. & Sutherland, S. (1993). Seasonal variation

- 1636 of CO₂ and nutrients in the high-latitude surface oceans: a comparative study. *Global*
1637 *Biogeochemical Cycles*, 7, 843–878. <https://doi.org/10.1029/93GB02263>
- 1638 Takahashi, T., Sutherland, S. C., Sweeney, C., Poisson, A., Metzl, N., Tillbrook, B., et al. (2002).
1639 Global sea-air CO₂ flux based on climatological surface ocean pCO₂, and seasonal biological and
1640 temperature effects. *Deep-Sea Research II*, 49, 1601–1622, [https://doi.org/10.1016/S0967-](https://doi.org/10.1016/S0967-0645(02)00003-6)
1641 [0645\(02\)00003-6](https://doi.org/10.1016/S0967-0645(02)00003-6)
- 1642 Takahashi, T., Sutherland, S. C., Wanninkhof, R., Sweeney, C., Feely, R. A., Chipman, D. W. et
1643 al.(2009). Climatological mean and decadal change in surface ocean pCO₂ and net sea-air CO₂ flux
1644 over the global oceans. *Deep-Sea Research II*, 56, 554–577,
1645 <https://doi.org/10.1016/j.dsr2.2008.12.009>
- 1646 Terhaar, J., Frölicher, T. L., & Joos, F. (2022). Observation-constrained estimates of the global
1647 ocean carbon sink from Earth system models. *Biogeosciences*, 19, 4431–4457.
1648 <https://doi.org/10.5194/bg-19-4431-2022>
- 1649 Terhaar, J., Goris, N., Müller, J.D., DeVries, T., Gruber, N., Hauck, J., Perez, F. & Séférian, R.
1650 ,2014. Assessment of Global Ocean Biogeochemistry Models for Ocean Carbon Sink Estimates in
1651 RECCAP2 and Recommendations for Future Studies. *Journal of Advances in Modeling Earth*
1652 *Systems*, 16, e2023MS003840. <https://doi.org/10.1029/2023MS003840>
- 1653 Thomas, H., Friederike Prowe, A. E., Lima, I. D., Doney, S. C., Wanninkhof, R., Greatbatch, R. J.,
1654 et al. (2008). Changes in the North Atlantic Oscillation influence CO₂ uptake in the North Atlantic
1655 over the past 2 decades. *Global Biogeochemical Cycles*, 22, GB4027,
1656 <https://doi.org/10.1029/2007GB003167>
- 1657 Tjiputra, J. F., Polzin, D., & Winguth, A. M. (2007). Assimilation of seasonal chlorophyll and
1658 nutrient data into an adjoint three-dimensional ocean carbon cycle model: Sensitivity analysis and
1659 ecosystem parameter optimization. *Global biogeochemical cycles*,
1660 *21*(1).<https://doi.org/10.1029/2006GB002745>
- 1661 Tjiputra, J. F., Assmann, K., & Heinze, C. (2010). Anthropogenic carbon dynamics in the changing
1662 ocean, *Ocean Sciences*, 6, 605–614. <https://doi.org/10.5194/os-6-605-2010>
- 1663 Tjiputra, J. F., Olsen, A., Assmann, K., Pfeil, B., & Heinze, C. (2012). A model study of the
1664 seasonal and long-term North Atlantic surface pCO₂ variability. *Biogeosciences*, 9, 907–923,
1665 <https://doi.org/10.5194/bg-9-907-2012>
- 1666 Tjiputra, J. F., Olsen, A. R. E., Bopp, L., Lenton, A., Pfeil, B., Roy, T., ... & Heinze, C. (2014).
1667 Long-term surface pCO₂ trends from observations and models. *Tellus B: Chemical and Physical*
1668 *Meteorology*, 66(1), 23083.<https://doi.org/10.3402/tellusb.v66.23083>
- 1669 Touratier, F., Goyet, C., Houpert, L., de Madron, X. D., Lefèvre, D., Stabholz, M., & Guglielmi, V.
1670 (2016). Role of deep convection on anthropogenic CO₂ sequestration in the Gulf of Lions
1671 (northwestern Mediterranean Sea). *Deep Sea Research Part I*, 113, 33–48.
1672 <https://doi.org/10.1016/j.dsr.2016.04.003>
- 1673 Ullman, D. J., McKinley, G. A., Bennington, V., & Dutkiewicz, S. (2009). Trends in the North
1674 Atlantic carbon sink: 1992–2006. *Global Biogeochemical Cycles*, 23(4).
1675 <https://doi.org/10.1029/2008GB003383>
- 1676 Urbini, L., Ingrosso, G., Djakovac, T., Piacentino, S. & Giani, M. (2020) Temporal and Spatial

- 1677 Variability of the CO₂ System in a Riverine Influenced Area of the Mediterranean Sea, the
1678 Northern Adriatic. *Front. Mar. Sci.* 7:679. <https://doi.org/10.3389/fmars.2020.00679>
- 1679 Vaittinada Ayar, P., Bopp, L., Christian, J. R., Ilyina, T., Krasting, J. P., Séférian, R., et al. (2022).
1680 Contrasting projections of the ENSO-driven CO₂ flux variability in the equatorial Pacific under
1681 high-warming scenario, *Earth System Dynamics*, 13, 1097–1118. [https://doi.org/10.5194/esd-13-](https://doi.org/10.5194/esd-13-1097-2022)
1682 [1097-2022](https://doi.org/10.5194/esd-13-1097-2022)
- 1683 Wanninkhof, R. (1992). Relationship between wind speed and gas exchange over the ocean.
1684 *Journal of Geophysical Research: Oceans*, 97(C5), 7373-7382. <https://doi.org/10.1029/92JC00188>
- 1685 Wanninkhof, R., Park, G. H., Takahashi, T., Sweeney, C., Feely, R., Nojiri, Y., et al. (2013). Global
1686 ocean carbon uptake: Magnitude, variability and trends. *Biogeosciences*, 10, 1983–2000.
1687 <https://doi.org/10.5194/bg-10-1983-2013>
- 1688 Wanninkhof, R. (2014). Relationship between wind speed and gas exchange over the ocean
1689 revisited. *Limnology and Oceanography: Methods*, 12(6), 351-
1690 362. <https://doi.org/10.4319/lom.2014.12.351>
- 1691 Wanninkhof, R., Pickers, P. A., Omar, A. M., Sutton, A., Murata, A., Olsen, A., et al. (2019). A
1692 Surface Ocean CO₂ Reference Network, SOCONET and Associated Marine Boundary Layer CO₂
1693 Measurements. *Frontiers in Marine Science*, 6:400. <https://doi.org/10.3389/fmars.2019.00400>
- 1694 Watson, A. J., Nightingale, P. D., & Cooper, D. J. (1995). Modelling atmosphere—ocean CO₂
1695 transfer. *Philosophical Transactions of the Royal Society of London. Series B: Biological Sciences*,
1696 348(1324), 125-132. <https://doi.org/10.1098/rstb.1995.0054>
- 1697 Watson, A. J., Schuster, U., Bakker, D. C., Bates, N. R., Corbière, A., González-Dávila, M., ... &
1698 Wanninkhof, R. (2009). Tracking the variable North Atlantic sink for atmospheric CO₂. *Science*,
1699 326(5958), 1391-1393. <https://doi.org/10.1126/science.1177394>
- 1700 Watson, A. J., Schuster, U., Shutler, J. D., Holding, T., Ashton, I. G., Landschützer, P., ... &
1701 Goddijn-Murphy, L. (2020). Revised estimates of ocean-atmosphere CO₂ flux are consistent with
1702 ocean carbon inventory. *Nature communications*, 11(1), 4422. [https://doi.org/10.1038/s41467-020-](https://doi.org/10.1038/s41467-020-18203-3)
1703 [18203-3](https://doi.org/10.1038/s41467-020-18203-3)
- 1704 Wilkin, J. L., Mansbridge, J. V., & Godfrey, J. S. (1995). Pacific Ocean heat transport at 24 N in a
1705 high-resolution global model. *Journal of physical oceanography*, 25(10), 2204-2214.
1706 [https://doi.org/10.1175/1520-0485\(1995\)025%3C2204:POHTAI%3E2.0.CO;2](https://doi.org/10.1175/1520-0485(1995)025%3C2204:POHTAI%3E2.0.CO;2)
- 1707 Wimart-Rousseau, C., Wagener, T., Álvarez, M., Moutin, T., Fourier, M., Coppola, L., ... &
1708 Lefèvre, D. (2021). Seasonal and interannual variability of the CO₂ system in the Eastern
1709 Mediterranean Sea: A case study in the north Western levantine basin. *Frontiers in Marine Science*,
1710 8, 649246. <https://doi.org/10.3389/fmars.2021.649246>
- 1711 Wallace, D. W. (2001). Storage and transport of excess CO₂ in the oceans: The JGOFS/WOCE
1712 global CO₂ survey. In *International Geophysics* (Vol. 77, pp. 489-L). Academic Press.
1713 [https://doi.org/10.1016/S0074-6142\(01\)80136-4](https://doi.org/10.1016/S0074-6142(01)80136-4)
- 1714 Woolf, D. K., Land, P. E., Shutler, J. D., Goddijn-Murphy, L. M., & Donlon, C. J. (2016). On the
1715 calculation of air-sea fluxes of CO₂ in the presence of temperature and salinity gradients. *Journal of*
1716 *Geophysical Research: Oceans*, 121(2), 1229-1248. <https://doi.org/10.1002/2015JC011427>
- 1717 Wright, R. M., Le Quéré, C., Buitenhuis, E., Pitois, S., and Gibbons, M. J. (2021). Role of jellyfish

- 1718 in the plankton ecosystem revealed using a global ocean biogeochemical model. *Biogeosciences*,
1719 18, 1291–1320, <https://doi.org/10.5194/bg-18-1291-2021>
- 1720 Yang, M., Bell, T. G., Bidlot, J.-R., Blomquist, B. W., Butterworth, B. J., Dong, Y., et al. (2022). Global
1721 Synthesis of Air-Sea CO₂ Transfer Velocity Estimates From Ship-Based Eddy Covariance Measurements.
1722 *Frontiers in Marine Science*, 9. Original Research.
1723 <https://www.frontiersin.org/articles/10.3389/fmars.2022.826421/full>
1724
- 1725 Zeng, J., Iida, Y., Matsunaga, T., & Shirai, T. (2022). Surface ocean CO₂ concentration and air-sea
1726 flux estimate by machine learning with modelled variable trends. *Frontiers in Marine Science*, 0-14.
1727 <https://doi.org/10.3389/fmars.2022.989233>
- 1728 Zunino, P., Pérez, F. F., Fajar, N. M., Guallart, E. F., Ríos, A. F., Pelegrí, J. L., & Hernández-
1729 Guerra, A. (2015). Transports and budgets of anthropogenic CO₂ in the tropical North Atlantic in
1730 1992–1993 and 2010–2011. *Global Biogeochemical Cycles*, 29(7), 1075–1091.
1731 <https://doi.org/10.1002/2014GB005075>